Expertise
and insight
for the future

Matti Semenuk

Torque Vectoring Development for Formula Student Vehicle

Helsinki Metropolia University of Applied Sciences

Bachelor of Engineering

Automotive Engineering

Thesis

31 May 2021

Tekijä(t) Otsikko Sivumäärä Aika	Matti Semenuk Torque Vectoring Development for Formula Student Vehicle 54 sivua 31.5.2021
Tutkinto	Insinööri (AMK)
Tutkinto-ohjelma	Ajoneuvotekniikka
Ammatillinen pääaine	Autosähkötekniikka
Ohjaaja	Erityisasiantuntija Petri Makkonen

Työn tavoitteena oli suunnitella torque vectoring- ja vetoluistonestojärjestelmä Metropolia Motorsportin tulevaan nelivetosähköautoon. Näiden järjestelmien tehtävänä on avustaa kuljettajaa ajoneuvon hallinnassa ja ohjauksessa. Koska kyseessä on kilpa-auto, tarkoituksena oli myös parantaa kierrosaikaa, jolla ajoneuvosta saataisiin kilpailukykyisempi.

Tämä työ aloitettiin tutkimalla torque vectoringin ja vetoluistoneston eri toteutustapoja ja niihin liittyviä ohjausjärjestelmiä. MATLAB Simulink -ohjelmointiympäristöön kehitettiin seitsemän vapausasteen ajoneuvomalli, jotta ohjausjärjestelmiä voitaisiin kehittää ja testata simuloinneissa.

Varsinainen ohjausjärjestelmän suunnittelu tehtiin MATLAB Simulink -ohjelmointiympäristössä. PID-säätimen säätämistä varten kehitettiin myös tila-avaruusmalli, jolla PID-säätimen parametreja voidaan säätää. Vetoluistoeston järjestelmää varten kehitettiin sumeaan logiikkaan perustuva säädin, joka rajoittaa pyörien luistoa kiihdytys- tai alhaisen pidon tilanteissa.

Järjestelmien testaaminen ja ajoneuvon simulointi tapahtui MATLAB Simulink -ohjelmointiympäristössä sekä IPG Carmaker -simulointiympäristössä. Pyörien rengasvoimien simuloinneissa käytettiin Pacejkan kehittämää Magic Formula -rengasmallia. Torque vectoring -järjestelmää simuloitiin askelvasteena sekä Autocross testissä. Vetoluistonestoa simuloitiin kiihdytystilanteessa, joka vastaa kilpailun Acceleration-osiota. Näiden testien tulokset esitellään työssä.

Työn tuloksena saatiin toimiva torque vectoring- ja vetoluistonestojärjestelmä, joka paransi kierrosaikaa simuloinneissa. Tulosten pohjalta esitettiin myös parannusehdotuksia jatkokehitystä varten.

Avainsanat	Torque vectoring, Vetoluistonesto, Formula Student, 7-vapausasteen ajoneuvomalli, Simulink, MATLAB

Author(s) Title Number of Pages Date	Matti Semenuk Torque Vectoring Development for Formula Student Vehicle 54 pages 31 May 2021
Degree	Bachelor of Engineering
Degree Programme	Automotive Engineering
Professional Major	Automotive Electronics Engineering
Instructor	Petri Makkonen, DSc (Tech.)

The aim of this thesis was to design baseline torque vectoring and traction control systems for the Metropolia Motorsport upcoming AWD electrical vehicle. The objective of these systems was to assist the driver in handling and steerability of a race car, and to increase vehicle lateral performance of the vehicle, and thus, reduce lap time.

The thesis was started by studying different torque vectoring and traction control systems, implementation strategies and different controller types for these systems. A 7DOF vehicle model was developed to test torque vectoring and traction control systems with MATLAB Simulink.

Control systems were developed in MATLAB Simulink simulation environment. To tune PID controller, state space model of linear single-track model was used to obtain PID controller gains. For traction control system fuzzy logic controller was developed to reduce wheel slip in acceleration or low friction situations.

Control systems and vehicle simulation was carried in MATLAB Simulink and in IPG Carmaker simulation environment. To simulate tire force, simplified Pacejka Magic Formula tire model was used. Torque vectoring system was simulated in step steer, Skidpad and Autocross tests. Traction control system was simulated in Acceleration event test. Results of these tests were briefly analyzed.

As a result of this thesis, working torque vectoring and traction control system were developed. Although vehicle was faster in simulations, real testing would need to be performed to validate simulation results. Also, few proposals for improving torque vectoring were discussed.

Keywords	Torque vectoring, Traction control system, Formula Student, 7-DOF vehicle model, Simulink, MATLAB

Contents

List of Abbreviations

A	Frontal area
C_f	Cornering stiffness at front
C_l	Coefficient of lift
C_r	Cornering stiffness at rear
CoG	Centre of Gravity
F_w	Viscous force of wheel
F_x	Longitudinal force of wheel
F_y	Wheel limited lateral force
F_z	Vertical tire force
F_{down}	Vehicle total produced downforce
F_{x0}	Tire longitudinal force
F_{x0}	Tire lateral force
F_{xfl}	Longitudinal force of front left wheel
F_{xfr}	Longitudinal force of front right wheel
F_{xrl}	Longitudinal force of rear right wheel
F_{xrr}	Longitudinal force of rear left wheel
F_{yfl}	Lateral force of front left wheel
F_{yfr}	Lateral force of front right wheel
F_{yrl}	Lateral force of rear left wheel
F_{yrr}	Lateral force of rear right wheel
G_r	Transmission gear ratio
I_{zz}	Moment of inertia around yaw axis
J_α	Wheel moment of inertia
K_u	Understeer gradient
M_z	Additional yaw moment
R	Radius of a turn
Re	Dynamic rolling radius of wheel
Td	Driving torque
α	Tire slip angle
α_f	Slip angle front
α_r	Slip angle rear
α_σ	Tire slip angle with relaxation
$\ddot{\psi}$	Vehicle yaw acceleration
δf	Steering wheel angle
$\dot{\omega}$	Wheel rotational acceleration
$\dot{\psi}$	Vehicle yaw rate
κ	Tire slip ratio
μ_x	Tire longitudinal coefficient of friction
ω_{FL}	Rotational velocity of front left wheel
ω_{FR}	Rotational velocity of front right wheel
ω_{RL}	Rotational velocity of rear left wheel
ω_{RR}	Rotational velocity of rear right wheel
σ	Tire relaxation length
a_x	Vehicle longitudinal acceleration
a_y	Vehicle lateral acceleration
h	Height of centre of gravity

l	Wheelbase
l_f	Distance from centre of gravity to front axle
l_r	Distance from centre of gravity to rear axle
m	Vehicle mass
m_f	Mass of a front axle
m_r	Mass of a rear axle
s_f	Track width front
s_r	Track width rear
v_w	Wheel velocity
v_x	Vehicle longitudinal velocity
v_y	Vehicle lateral velocity
w_f	Half of track width front
w_r	Half of track width rear

Glossary

DOF	Degrees of freedom
ESC	Electronic stability control
FSAE	Formula SAE
FX-SR	Longitudinal force - slip ratio curve
ICE	Internal combustion engines
PID	Proportional-integral-derivative controller
TTC	Tire Test Consortium

1 Introduction

Metropolia Motorsport designs and manufactures a racecar every year to compete the Formula Student-class races. The team was established in 2000 to compete in combustion class and from year 2013 the team has been developing only electrical race cars.

The 6th electrical racecar HPF019 of Metropolia Motorsport uses two inboard electric motors to power the rear axle. Pros of this can kind of a powertrain are its simple design and easy maintenance. Cons of this kind of a setup have been relatively high usage of space and weight of the powertrain. The problem with this kind of a powertrain has been a loss of traction at acceleration and the vehicle's oversteering behavior. In addition, if these motors are not controlled individually, they can act as a locking differential to keep the wheels rotating at the same speed and can create tire scuffing.

The goal Metropolia Motorsport is to continuously develop and improve their own racecars to stay at competitive level. The team has set up a goal to design a four-wheel drive electric racecar for season 2021. This goal could be achieved with using four outboard motors with planetary gear reduction integrated in uprights.

This kind of configuration opens possibilities to create a torque vectoring system to achieve higher lateral performance of the vehicle and better stability and handling without altering longitudinal performance. The traction control system can also be developed to be more precise and faster with electric motors than traditional TCS used in combustion vehicles.

Many Formula Student teams have proved that by using torque vectoring and four-wheel drive race cars it is possible to achieve higher lateral performance from the vehicle and win competitions.

1.1 Formula Student

Formula Student is an international student engineering competition. The objective is to design and manufacture a single-seat Formula Student race car to compete in international competitions. This competition is divided into three classes: combustion, electrical, and driverless classes. For these competitions there are guidelines which every team must follow strictly to pass the inspections and to be able to participate in the competitions. These competitions are divided into dynamic and static parts.

The dynamical part of the competition is divided in four driving events which are the following [1]:

- skidpad
- acceleration
- autocross
- endurance.

And the static part of competition is divided into three parts which are the following:

- design
- cost
- business plan.

1.2 HPF021

HPF021 is the newest electric vehicle in developing. Figure 2 shows the concept design of the vehicle.

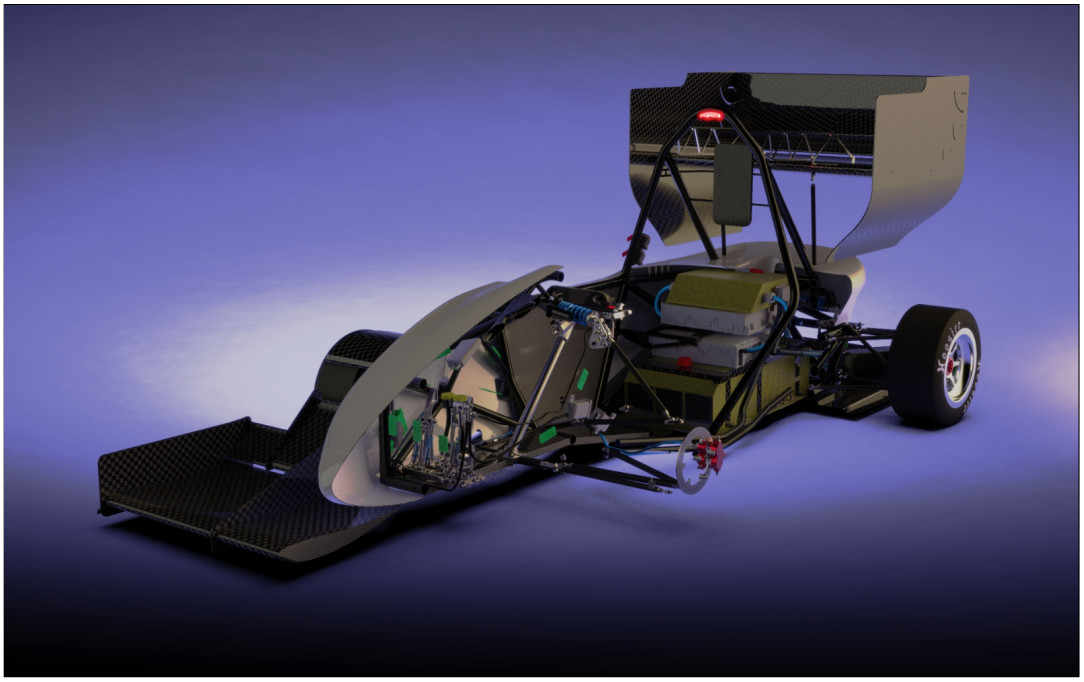

Figure 1: Concept picture of Metropolia Motorsport HPF021 vehicle

The design of new vehicle was started in fall 2019. The starting point for the new vehicle design was moving vehicle from a rear-wheel driven to an all-wheel drive vehicle. After competition, the vehicle will be first four-wheel driven vehicle of Metropolia Motorsport. The vehicle is planned to be finished for the year 2021 competitions. It is also planned to be equipped with four electric motors produced by Fischer Elektromotoren GmbH. Due to high RPM of motors and low torque it is planned to use reduction gear to achieve balance between acceleration and top speed. The motors and planetary gearboxes are planned to be integrated in wheel uprights. Vehicle features high-strength steel tube space frame with composite side impact structures. Suspension is designed to be equipped with double wishbone suspension setup.

The technical specifications of the vehicle are listed in table 1. The vehicle parameters are listed in table 2.

Table 1: Technical specifications HPF021

0 - 100 km/h	< 3 s
Top speed	120 km/h
Cell	Melasta SLPBB042126
Tires	Hoosier LC0 10”
Gearbox	4 Planetary gear box
Motor	4 Fischer TI085-052-070-04B7S-07S04BE2 electric motors

Table 2: Vehicle parameters HPF021

Parameter	Value	Unit
Mass	280	[Kg]
Wheelbase	1530	[mm]
Track width front	1200	[mm]
Track width rear	1200	[mm]
Centre of height	30	[mm]
Tire dynamic rolling radius	205	[mm]
Moment of inertia around z axis	180	[kgm^2]
Gear ratio	12	[-]
Wheel inertia	0.8	[kgm^2]
Steering gear ratio	5	[-]
Frontal area of vehicle	1.2	[m^2]
Coefficient of drag	1.23	[-]
Coefficient of lift	3.7	[-]

1.3 Project Goal

The goal of this thesis was to develop a baseline torque vectoring system which will increase the lateral performance of the vehicle in cornering situations without affecting vehicle longitudinal performance. This performance is measured in lap times on the track. Torque vectoring uses a high-level controller to create additional yaw moment and a low-level controller which translates this yaw moment to wheel torques. To eliminate wheel slip in acceleration and cornering situations, traction control system was also developed.

2 Vehicle Dynamics

Vehicle dynamics is a branch of vehicle mechanics that tries to describe how a vehicle will behave in motion to set inputs and disturbances. Usually, vehicle modelling and simulation is a complex and difficult task. Vehicle models are only mathematical models to describe how vehicle behaves which tries to represent the real system as closely as possible. These mathematical models can vary from linear single-track models to multi-body systems. Vehicle model can be divided to its components which are the following [2, p. 1 - 4]:

- wheel suspension
- chassis
- seats
- wheels
- drivetrain
- packaging
- steering
- brakes
- auxiliary components.

Specific software can be used to deal with non-linearity on varying level of formalism e.g. walking body dynamics or block systems, for example ADAMS or IPG Carmaker. Often when simulating vehicle dynamics control systems, a vehicle model with seven degrees of freedom is used. The advantage of this model is relatively easy simulations that do not require multi-body simulation tools. A seven degree of freedom vehicle model is shown Figure 2.

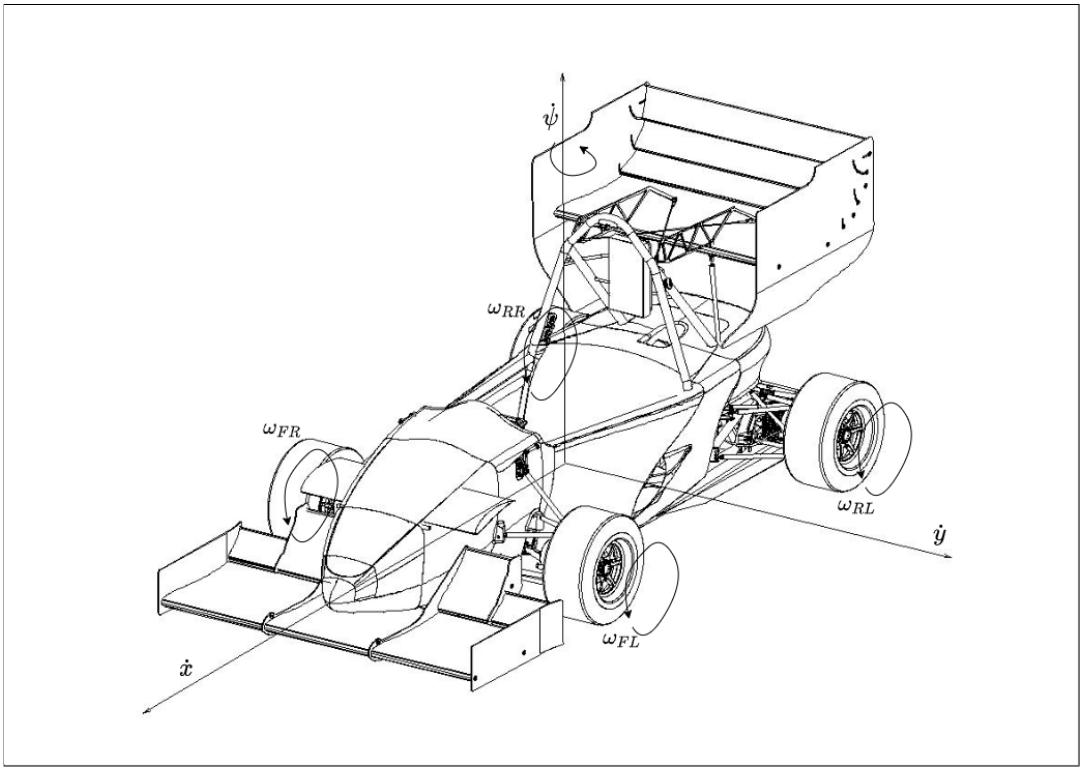

Figure 2: Degrees of freedom in vehicle model

From this figure the following degrees of freedom can be written:

- v_x vehicle longitudinal velocity
- v_y vehicle lateral velocity
- $\dot{\psi}$ vehicle yaw rate
- ω_{FL} front left wheel rotational velocity
- ω_{FR} front right wheel rotational velocity
- ω_{RL} rear left wheel rotational velocity
- ω_{RR} rear right wheel rotational velocity.

2.1 Vehicle Body Equations

A vehicle body model is used with three degrees of freedom which is shown in Figure 3.

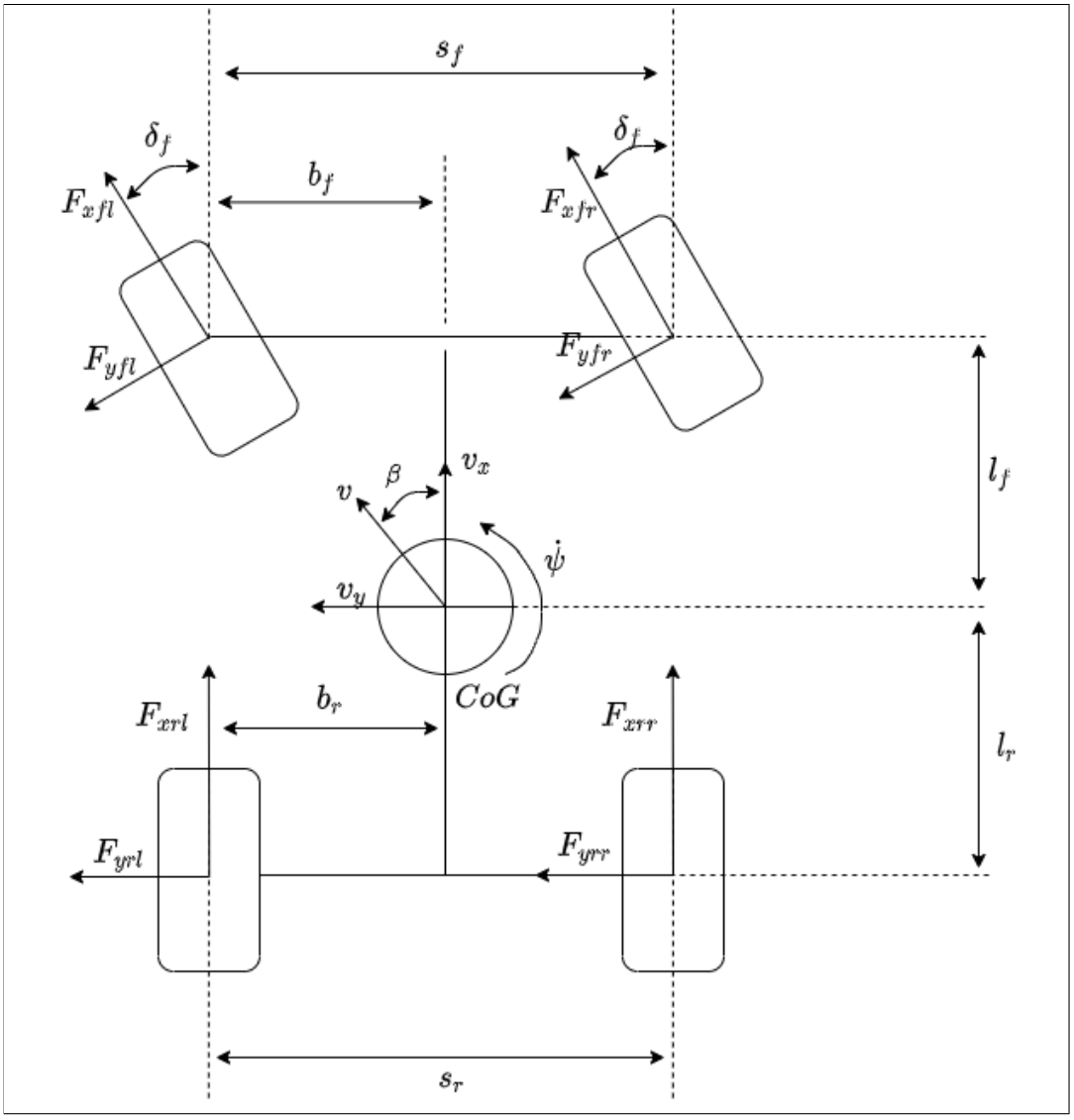

Figure 3: Degrees of freedom in vehicle model

Pitch and roll motions of the vehicle are neglected. Angle of front wheels is given by the steering wheel angle. Vehicle mass is assumed to be at the centre of gravity. From this the following equations can be written in the reference frame of the vehicle. Fx, Fy are forces produced by wheels. Steering wheel angle at front wheels is given by δ_f. Equations according to Newton-Euler can be written as [3, p. 1309.]:

$$m(a_x - v_y\dot{\psi}) = F_{xfl}cos(\delta_f) - F_{yfl}sin(\delta_f) + F_{xfr}cos(\delta_f) - F_{yfr}cos(\delta_f) + F_{xrl} + F_{xrr} \quad (1)$$

$$m(a_y + v_x\dot{\psi}) = F_{xfl}sin(\delta_f) + F_{yfl}cos(\delta_f) + F_{xfr}sin(\delta_f) + F_{yfr}cos(\delta_f) + F_{yrl} + F_{yrr} \quad (2)$$

$$\ddot{\psi} I_{zz} = l_f(F_{xfl}sin(\delta_f) + F_{xfr}sin(\delta_f) + F_{yfl}cos(\delta_f) + F_{yfr}cos(\delta_f)) + w_f(-F_{xfl}cos(\delta_f) + F_{xfr}cos(\delta_f) + F_{yfl}sin(\delta_f) - F_{yfr}sin(\delta_f)) - lr(F_{yrl} + F_{yrr}) - w_r(F_{xrl} + F_{xrr}) \quad (3)$$

where v_x, v_y are vehicle longitudinal and lateral velocities acting at the centre of mass, $\dot{\psi}$ is vehicle yaw rate, w_f and w_r are lateral distances from vehicle centre of gravity to the left and the right wheels respectively and l_f, l_r are distances from centre of gravity to the front and the rear axle respectively.

2.2 Wheel Loads

Vertical tire forces of the vehicle determine the vehicle's ability to deliver torque to road for the vehicle. To calculate vertical tire forces, tire statical load, load transfer and the aerodynamic downforce are taken into calculations.

Statical vertical tire forces are given by mass on each vehicle, when the vehicle is in resting state. This usually depends on overall weight distribution between the front and the rear axle and is given by following equations [3, p. 1311.]:

$$Fz_0, f = \frac{mgl_r}{l} \quad (4)$$

$$Fz_0, r = \frac{mgl_f}{l} \quad (5)$$

where Fz_0, f, Fz_0, r are weight of the front and the rear axle, m is vehicle mass and g is gravitational acceleration.

Lateral load transfer results from tire lateral forces that act on the vehicle centre of gravity by creating lateral acceleration. This lateral acceleration shifts the overall mass of the vehicle from the inner wheels to the outside wheels. If vehicle roll motion and suspension

geometry are neglected, the total lateral load transfer comes strictly from lateral acceleration and is given by the following equation:

$$Fz_{a_y} = \frac{mha_y}{s} \tag{6}$$

where Fz_{a_y} is total lateral load transfer, a_y is lateral acceleration of the vehicle, s is front or the rear track width and h is height of the centre of gravity.

During acceleration or braking the vehicle undergoes the same similar kind of load transfer as in lateral acceleration. These longitudinal forces act at the centre of gravity to create longitudinal acceleration to accelerate or brake the vehicle. If vehicle suspension geometry and pitch motion are neglected, total longitudinal load transfer is given by the following equation:

$$Fz_{a_x} = \frac{mha_x}{l} \tag{7}$$

where Fz_{a_x} is total load transfer expressed in Newtons, a_x is longitudinal acceleration of the vehicle.

Negative lift, or as it often called downforce, is aerodynamical force which acts on a vehicle and is dependent on many factors. In race cars downforce plays a crucial role by increasing vertical tire forces of the vehicle and increases lateral performance of the vehicle in cornering situations. Mostly this force depends on lift coefficient and speed of the vehicle. Simulations of the vehicle aerodynamical properties is a complex task and many CFD simulation tools have been created to help with obtaining results. For easier calculations often coefficient of lift and air density are estimated to remain constant. This downforce is estimated to split evenly to all four wheels. By making these assumptions vehicle downforce can be calculated by the following equation [4, p. 47.]:

$$F_{down} = \frac{1}{2}\rho C_l A v_x^2 \tag{8}$$

where F_{down} is total produced vehicle downforce, ρ is air density, C_l is vehicle coefficient of lift and v_x longitudinal velocity of the vehicle. These equations can be combined to write the final equations for vertical tire forces.

$$Fz_{fl} = \frac{1}{2}Fz_0, f - \frac{1}{2}Fz_{ax} + \frac{1}{2}Fz_{ay} + \frac{1}{4}F_{down} \tag{9}$$

$$Fz_{fr} = \frac{1}{2}Fz_0, f - \frac{1}{2}Fz_{ax} - \frac{1}{2}Fz_{ay} + \frac{1}{4}F_{down} \tag{10}$$

$$Fz_{rl} = \frac{1}{2}Fz_0, r + \frac{1}{2}Fz_{ax} + \frac{1}{2}Fz_{ay} + \frac{1}{4}F_{down} \tag{11}$$

$$Fz_{rr} = \frac{1}{2}Fz_0, r + \frac{1}{2}Fz_{ax} - \frac{1}{2}Fz_{ay} + \frac{1}{4}F_{down} \tag{12}$$

2.3 Tire Modelling

Tires are the only component that comes to contact with road in the vehicle. This means that tires are the most safety critical feature in a vehicle. Tires have to carry the mass of the vehicle, to bring ride comfort and to transmit force in all three dimensions. Tires are also key factors in stability and handling capabilities of the vehicle. Tire properties depends on many factors, such as [5]:

- tire material
- tire thread pattern
- tire pressure
- tire temperature
- road temperature
- tire normal force
- tire wear level.

Figure 4 shows longitudinal force - slip ratio curve.

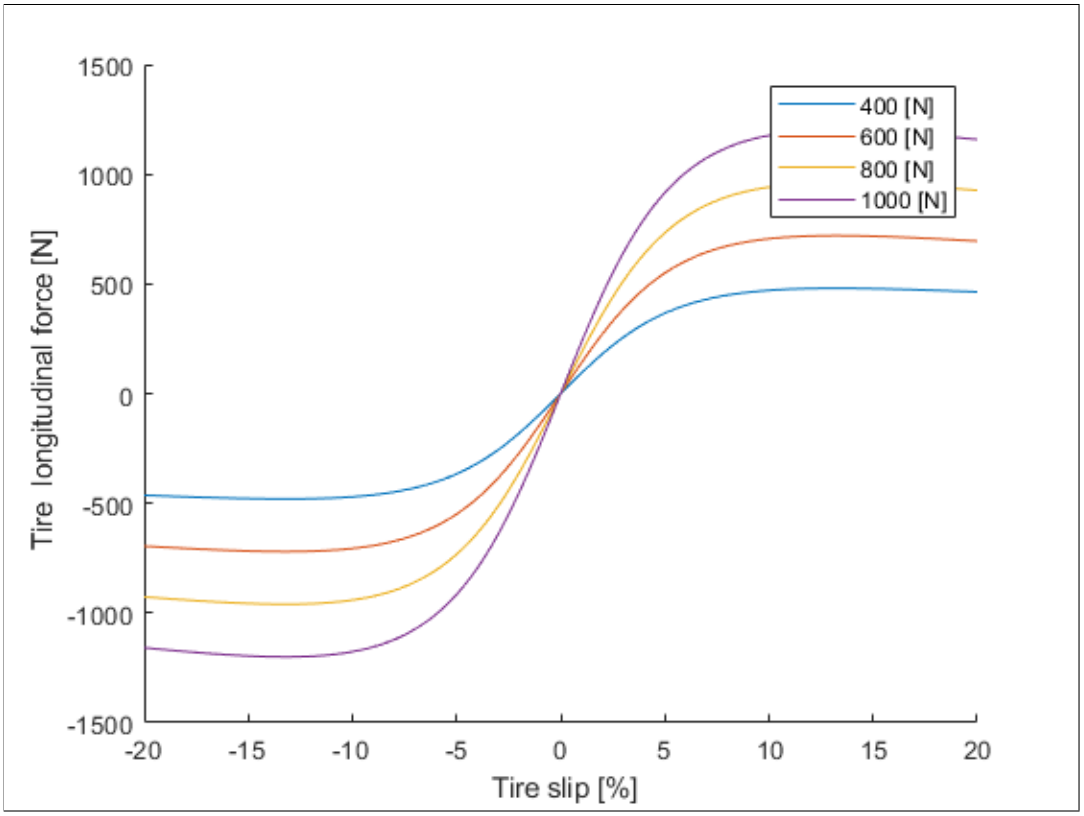

Figure 4: Longitudinal force produced by tire based on current slip and normal force of tire

From this figure it can be seen that tire transmitted force rises as slip is increasing. However, this relationship is not linear as slip is increasing. Usually, the peak force is reached between 10 - 30 %. This peak value heavily depends on the road surface and on slippery surfaces the peak can be at around 30 %. For this reason, many tire models were developed to describe tire behavior beyond linear range. The most widely and commonly used tire model was developed by Hans B. Pacejka, and it is called Magic Formula tire model [6].

2.4 Pacejka's Magic Formula Tire Model

Magic Formula is a semi-empirical tire model. This means that the measured tire data are fitted to the Magic Formula model. From this the Magic Formula coefficients can be obtained which are called B, C, D and E. A simplified Magic formula model is given by the following equations for pure longitudinal or lateral slip situations [3, p. 1309.]:

$$F_{x0} = \mu_x F_z sin(C_x arctan(B_x k - E_x(B_x k - arctan(B_x k)))) \quad (13)$$

$$F_{y0} = \mu_y F_z sin(C_y arctan(B_y \alpha - E_y(B_y \alpha - arctan(B_y \alpha)))) \quad (14)$$

where μ_x , μ_y is the longitudinal and lateral friction coefficient of the tires, α is tire slip angle, κ is tire slip ratio, B, C, D and E are the Magic Formula coefficients for a fitted tire.

Tire can produce peak lateral force only in driving situations, where longitudinal force is not produced. The same applies for longitudinal driving situations, in which the tire is able to produce peak longitudinal force, if the lateral force is not presented. This situation can be seen when looking at the vehicle g-g diagram. The vehicle g-g diagram shows the vehicle's ability to produce lateral and longitudinal acceleration. This corresponds to the vehicle's performance. For example, by increasing vehicle's lateral acceleration limit a_y, it possible to achieve higher velocity during cornering by the following equation $a_y = \frac{v^2}{R}$ where R is corner radius. Figure 5 shows an actual g-g diagram taken from the Autocross event during the FS East competition.

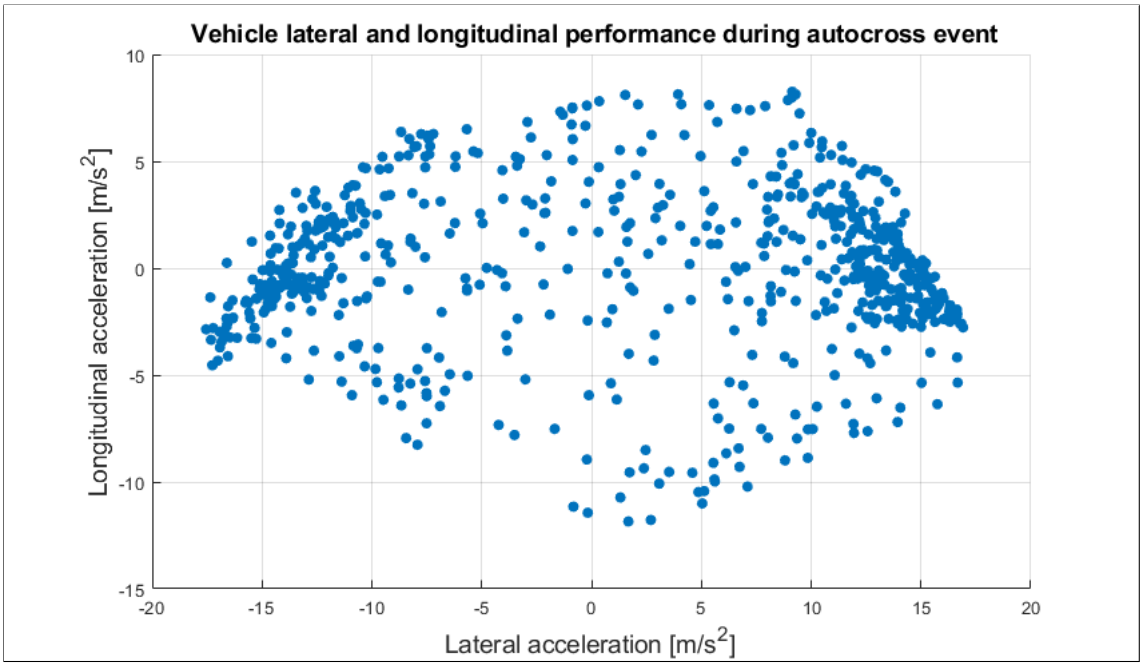

Figure 5: g-g diagram from HPF019 vehicle data

In the figure above it can be clearly seen that the vehicle produced peak lateral accel-

eration when longitudinal acceleration is close or equals to zero. The same applies for situations where peak longitudinal acceleration was obtained. The x-axis is showing lateral acceleration and the y-axis longitudinal acceleration. For these reasons the combined tire force model based on friction ellipse can be used to get more realistic results from the tire model. This equation is given by the following equation [7]:

$$F_y = F_{y0}\sqrt{1 - (\frac{F_{x0}}{\mu_x F_z})^2} \tag{15}$$

where F_y is limited lateral force and F_z is tire normal force.

Tire slip ratio is defined as the ratio between vehicle velocity and the driven wheel velocity and is given by the following equation [8, p. 65.]:

$$\kappa = -\frac{v_x - R_e\omega}{v_x} \tag{16}$$

where κ is wheel current slip ratio, R_e is wheel dynamic rolling radius and ω is wheel rotational velocity.

Slip angle is the angle between wheel longitudinal velocity vector and the sum of longitudinal and lateral velocity vectors and is given by the following equation [8, p. 67.]:

$$\alpha = -tan^{-1}\frac{v_y}{v_x} \tag{17}$$

where v_y is wheel lateral velocity and v_x is wheel longitudinal velocity.

With slip angles, tire transient behaviour needs to be accounted for, as tires cannot develop full lateral force straight away. To calculate tire transient response, tire relaxation length is taken into account. Relaxation length is a distance, which the tire rolls before lateral force is developed to 65 % of its steady-state value. This relaxation length is taken into account by the following equation:

$$\alpha_\sigma = \frac{1}{s}\left[\frac{(\alpha - \alpha_\sigma)V_w}{\sigma}\right] \tag{18}$$

where α_σ is tire slip angle with relaxation length, σ is relaxation length and v_w is wheel current longitudinal velocity.

2.5 Wheel Dynamics

Figure 6 shows free body diagram of a driven wheel.

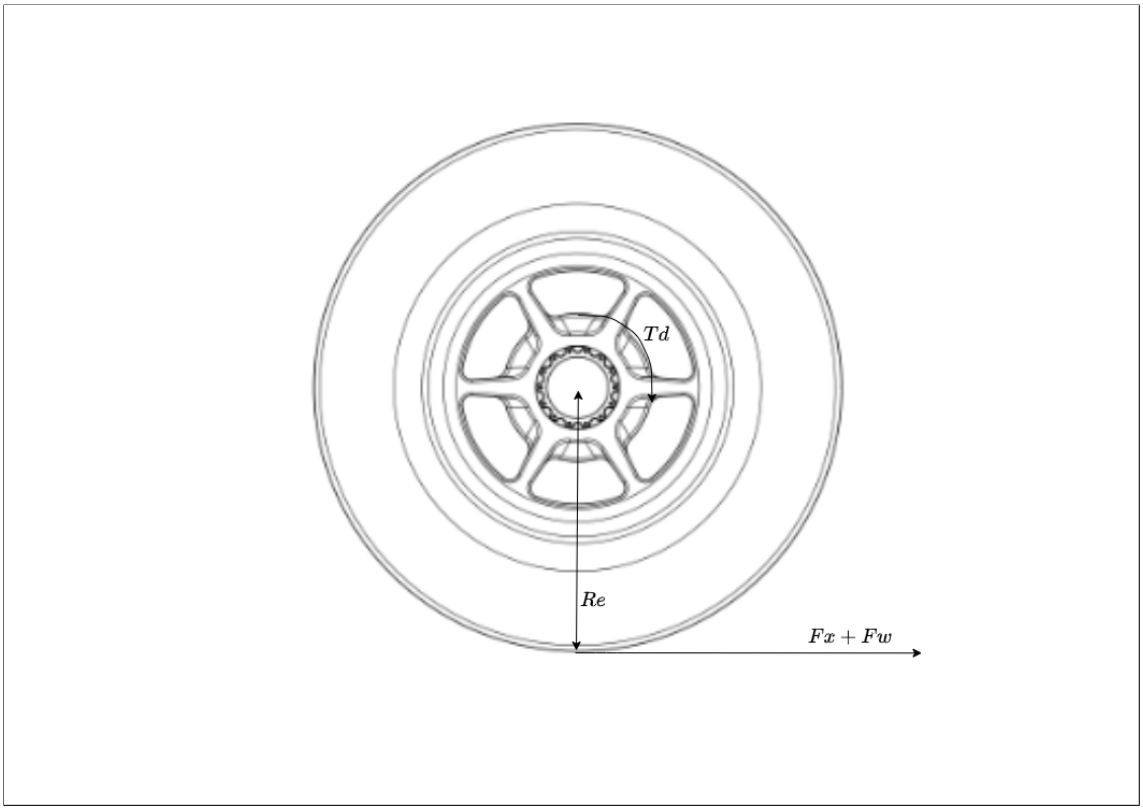

Figure 6: Free body diagram of wheel

From the figure above the wheel angular acceleration can be calculated by angular motion of the wheel.

$$Jw\dot{\omega} = T_d - R_e Fx - R_e F_w \tag{19}$$

where $J\alpha$ is wheel moment of inertia, $\dot{\omega}$ is wheel rotational velocity, F_x is wheel longitudinal force and F_w is the force caused by wheel viscous friction.

Figure 7 shows overall vehicle model which is implemented in MATLAB/Simulink.

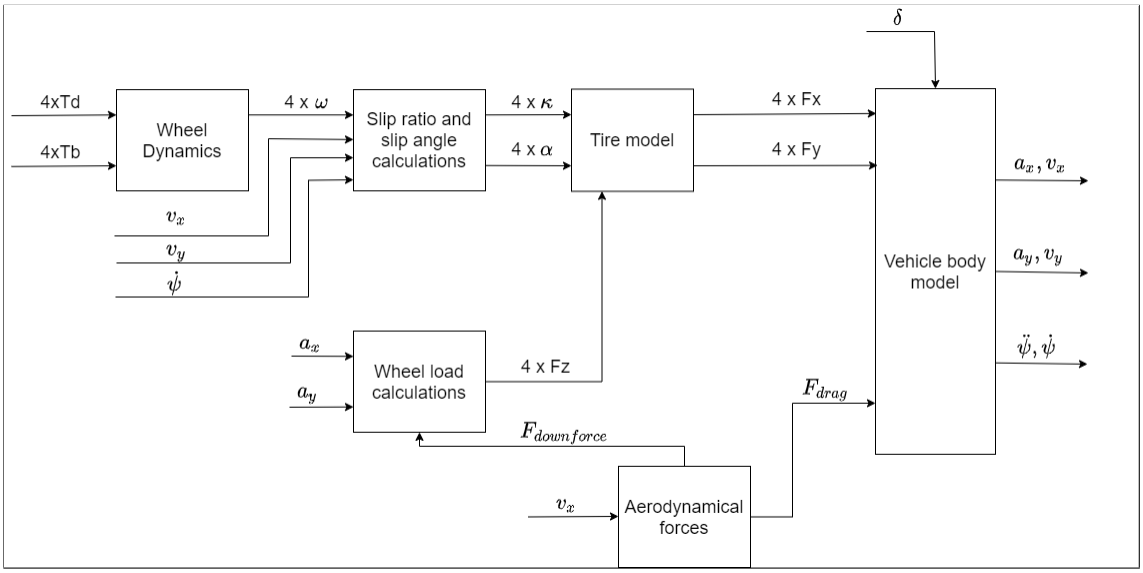

Figure 7: Overall vehicle model implemented in Simulink

This vehicle model can be used to test the torque vectoring system and to tune controller gains.

2.6 Linear Single-track Model

Vehicle lateral dynamics can be also studied with a linear single-track model. This model is often used to design lateral and yaw dynamic control systems. To get linear representation of a single-track model few assumptions are made:

- wheels on axle are lumped together
- heave, roll, pitch motions are neglected
- tire forces are estimated to be linear
- tire aligning torque is ignored
- tire slip angles are estimated to be small
- additional yaw moment is modeled by M_z
- vehicle longitudinal velocity is assumed to be constant
- aerodynamic force and torques are neglected.

The equations of motion for a single track-model are given by [9, p. 163.]:

$$m(a_y + \dot{\psi} v_x) = F_{xf} cos(\delta) + F_{xr} - F_{yf} sin(\delta) \tag{20}$$

$$I_{zz} \dot{\psi} = l_f F_{xf} sin(\delta) + l_f F_{yf} cos(\delta) - l_r F_{yr} \tag{21}$$

where I_{zz} is moment of inertia around the z-axis of the vehicle.

Slip angles of single-track models are given by the following equations:

$$\alpha_f = \delta - tan^{-1} \frac{v_y + l_f \dot{\psi}}{v_x} \tag{22}$$

$$\alpha_r = -tan^{-1} \frac{v_y - l_r \dot{\psi}}{v_x} \tag{23}$$

By linearizing equations 20 and 21 we get following differential equations:

$$a_y = \dot{\psi} \frac{1}{m}(-v_x m - \frac{C_f l_f}{v_x} + \frac{C_r lr}{v_x}) - v_y \frac{1}{m}(\frac{C_f}{v_x} + \frac{C_r}{v_x}) + \frac{C_f}{m}\delta \tag{24}$$

$$\ddot{\psi} = \dot{\psi} \frac{1}{I_{zz} v_x}(-l_f^2 C_f - l_r^2 C_r) + v_y \frac{1}{I_{zz} v_x}(l_f C_f - l_r C_r) + M_z \frac{1}{I_{zz}} + \delta \frac{l_f C_f}{I_{zz}} \tag{25}$$

2.7 State Space Model

Previous differential equations can be also represented in state space form. General state-space representation of linear system is given by:

$$\dot{x} = Ax + Bu \tag{26}$$

$$y = Cx + Du \tag{27}$$

For state variables the vehicle lateral velocity and yaw rate are selected:

$$\begin{bmatrix} v_y \\ \dot{\psi} \end{bmatrix}$$

With this following linear state space model for linear single-track model can be obtained:

$$\begin{bmatrix} \dot{v_y} \\ \ddot{\psi} \end{bmatrix} = \begin{bmatrix} \frac{-(C_r+C_f)}{mv_x} & \frac{(-{v_x}^2 m-C_f l_f+C_r l_r)}{mv_x} \\ \frac{(l_r C_r-l_f C_f)}{I_{zz} v_x} & \frac{({l_f}^2 C_f-{l_r}^2 C_r)}{I_{zz} v_x} \end{bmatrix} \begin{bmatrix} v_y \\ \dot{\psi} \end{bmatrix} + \begin{bmatrix} \frac{C_f}{m} & 0 \\ \frac{l_f C_f}{I_{zz}} & \frac{1}{I_{zz}} \end{bmatrix} \begin{bmatrix} \delta \\ M_z \end{bmatrix}$$

This model can be used to study the vehicle's lateral dynamics and to design controllers for the vehicle yaw motion and the vehicle's lateral dynamics.

3 Torque Vectoring

Vehicle stability can be measured usually with two quantities. Vehicle slip angle is usually denoted by β and vehicle yaw rate by $\dot{\psi}$. Vehicle slip angle is a difference between the direction where the vehicle is travelling and the direction in which the vehicle body is pointing. With positive slip angle values the vehicle is said to be understeering. With negative slip angle values the vehicle is said to be oversteering. Yaw rate is the vehicle current rotational velocity around its z-axis. With high yaw rate values, the vehicle tends to be highly unstable, and could spin from the desired course. With small values of yaw rate the vehicle has a reduced ability to follow the desired course which can also result in deviate from the desired course. These values can be monitored and modified with the torque vectoring system.

The objective of torque vectoring is to distribute braking and driving forces between wheels. This creates additional yaw moment which can increase the yaw acceleration usually for performance or decrease it for stability. This additional yaw moment can be created by different components, such as:

- braking individual wheels
- torque vectoring differentials
- front to rear torque distribution
- wheel specific electric motors.

Passive torque vectoring system is a system, where the individual wheels are braked to create additional yaw moment. This system is usually easiest to implement, if the vehicle has already an ESC system. Downside of this kind of a system is decreased lateral performance as the vehicle loses longitudinal velocity when the system is activated [10].

Mechanical torque vectoring can be done through active differentials. In this case engine torque is split through differential to the left and the right wheel. Usually, this kind of setup has a set of clutches to create asymmetric torques between the left and the right wheels. If more torque is given to the outside wheels the vehicle tends to oversteer, and if more

torque is given to the inner wheels, the vehicle tends to understeer [11]. Usually, this kind of torque vectoring does not affect the vehicle's longitudinal performance, and thus, is better than passive torque vectoring system. Downside of this kind of system is the high cost of implementation and the complex structure of differentials.

Electrical torque vectoring can be implemented in a vehicle with two electric motors on one axle or four electric motors on two axles. With four electric motors the torque can be easily controlled between the front and the rear axle and between the left and the right wheels. Electric motors have also faster response than ICE vehicles. These electric motors can also act as generators by creating torque in opposing direction.

3.1 Yaw Rate Reference

When vehicle behavior is analyzed in steady state cornering, the following relationship can be written between vehicle steering angle and turn radius. This equation is given by [12, p. 56.]:

$$\delta = \frac{l}{R} + K_u \frac{{v_x}^2}{R} \tag{28}$$

where K_u is vehicle understeer gradient.

Understeer gradient determines the vehicle's a understeering or oversteering behavior and is given as a difference between the front axle cornering stiffness to the front axle mass ratio and the rear axle cornering stiffness to the rear axle mass ratio [12, s. 57.].

$$K_u = \frac{m_f}{C_f} - \frac{m_r}{C_r} \tag{29}$$

In case of understeering, K_u gets positive values. In other words, to stay on the desired course vehicle steering wheel angle has to be increased, when lateral acceleration of the vehicle is increasing.

$$K_u = \frac{m_f}{C_f} > \frac{m_r}{C_r} \rightarrow K_u > 0 \rightarrow \alpha_f > \alpha_r \tag{30}$$

In case of oversteering, K_u gets negative values. In other words, to stay on the desired course vehicle steering wheel angle has to be decreased, when vehicle lateral acceleration is increasing.

$$K_u = \frac{m_f}{C_f} < \frac{m_r}{C_r} \rightarrow K_u < 0 \rightarrow \alpha_f < \alpha_r \tag{31}$$

In case of neutral steering, K_u value equals to zero. In other words, to stay on the desired course the steering wheel angle has to stay the same, when lateral acceleration is increasing.

$$K_u = \frac{m_f}{Cf} = \frac{m_r}{Cr} \rightarrow K_u = 0 \rightarrow \alpha_f = \alpha_r \tag{32}$$

With these equations it can be concluded that if the vehicle is neutral-steered it can have the smallest possible turning radius in constant radius turn. To have most performance out of the vehicle a neutral-steering approach should be chosen. However,based on driver preferences and better handling, a different approach was taken. The idea was to have oversteering behaviour at slow turns and understeering behaviour at fast turns. Oversteering behaviour at slow turns would help with turning into a corner faster and understeering at fast turns will help with handling of the vehicle.

In steady state cornering geometric yaw rate can be written as:

$$\dot{\psi}_{reference} = \frac{v_x}{R} \tag{33}$$

where v_x is vehicle longitudinal velocity and R is radius of turn.

This geometric yaw rate is taken as a reference which the vehicle has to follow to remain as close as possible to desired course. Equation 28 can be rewritten as a turning radius:

$$\frac{1}{R} = \frac{\delta}{l + K_u {v_x}^2} \tag{34}$$

Equations 33 and 34 can be combined to write reference yaw rate as function of the vehicle's longitudinal velocity and steering wheel angle.

$$\dot{\psi}_{reference} = \frac{V_x}{l + K_u {v_x}^2}\delta \tag{35}$$

In this equation K_u is a tunable variable for each driver preference which varies according to speed. This yaw rate reference will be used as a reference which vehicle yaw rate has to follow.

3.2 Maximum Yaw Rate Reference

In some cases, the desired yaw rate reference cannot be achieved due low friction coefficient situations. In this situation, the tires cannot generate the required amount of force to achieve the desired yaw moment. In this case the maximum value of yaw rate reference has to be restricted.

Maximum yaw rate reference is limited by lateral friction coefficient and the vehicle's current longitudinal velocity by the following equation [12, s. 212]

$$\dot{\psi}_{limit} = \frac{\mu g}{v_x} \tag{36}$$

where μ is road-tire coefficient of friction.

Yaw rate reference is passed to controller as long as it does not exceed yaw rate reference limit value. In case yaw rate reference exceeds the yaw rate limit, the yaw rate reference is limited by the following equation:

$$\dot{\psi}_{desired} = \begin{cases} \dot{\psi}_{reference}, & if \quad |\dot{\psi}_{reference}| < \dot{\psi}_{limit} \\ \dot{\psi}_{limit}, & if \quad |\dot{\psi}_{reference}| > \dot{\psi}_{limit} \end{cases} \tag{37}$$

3.3 Control Design

In many cases torque vectoring is used to enhance vehicle handling and stability. This is done through control of vehicle slip angle β and yaw rate $\dot{\psi}$. In many cases vehicle stability is controlled by making sure that vehicle slip angle value is small. This ensures that handling of the vehicle remains possible. Disadvantages of this kind of a system is that measuring this slip angle is expensive. Often this slip angle is estimated via an estimator. In our case slip angle estimation or measurement was not possible. For this reasons vehicle slip angle is assumed to remain zero to reduce complexity of the control system.

In our case only yaw rate of the vehicle was taken into consideration when designing the control system for the vehicle. The idea is to increase or lower the vehicle's yaw rate acceleration to achieve better lateral performance in cornering situations. This is done by controlling four electric motor torques to create additional yaw moment M_z.

3.4 Control Law

Many different control laws have been designed for torque vectoring control. This control law can be as simple as distributing torque based on steering wheel angle. Equation 38 shows yaw moment distribution based on steering wheel angle.

$$M_z = k\delta \tag{38}$$

where δ is steering wheel angle and k is system gain.

Usually, this kind of a system is not preferred due to high possibility of excess yaw rate

gain which can lead to vehicle instability. Feed forward controllers are often not used as system stability cannot monitored. Usually, the gain k is scheduled with the help of vehicle longitudinal v_x to achieve better controller performance. Open loop controllers will often require low computational effort and are fast. Downsides of the open loop controller is poor response to disturbances, for example road friction of coefficient and model variation parameters. There is also a possibility to achieve too aggressive yaw response and it will lead to decreased vehicle stability.

To achieve better controller performance closed loop controllers are often used in the torque vectoring system. PID type of controller is a widely used controller. It has straightforward implementation and it is often used in the torque vectoring system. Some torque vectoring systems use for example sliding mode control, Fuzzy control, robust control or optimal control systems. Every control system has its own advantages and disadvantages.

In our case open loop and closed loop controller were planned to be used in parallel. The objective of the close loop controller is to eliminate error between reference yaw rate and measured yaw rate. Feed forward control, based on equation 38 is also used with closed loop controller to control vehicle understeering or oversteering behavior depending on vehicle velocity.

The overall controller structure is shown in figure 8.

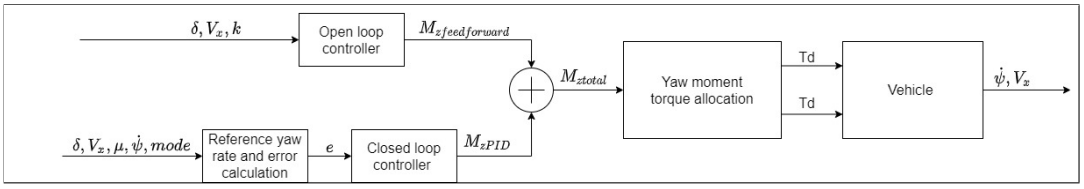

Figure 8: HPF021 controller structure

The state space model was analyzed in frequency and time domain. First this vehicle step response was analyzed at different velocities. Figure 9. shows the vehicle response from yaw moment to yaw rate when 1 Nm of yaw moment is applied.

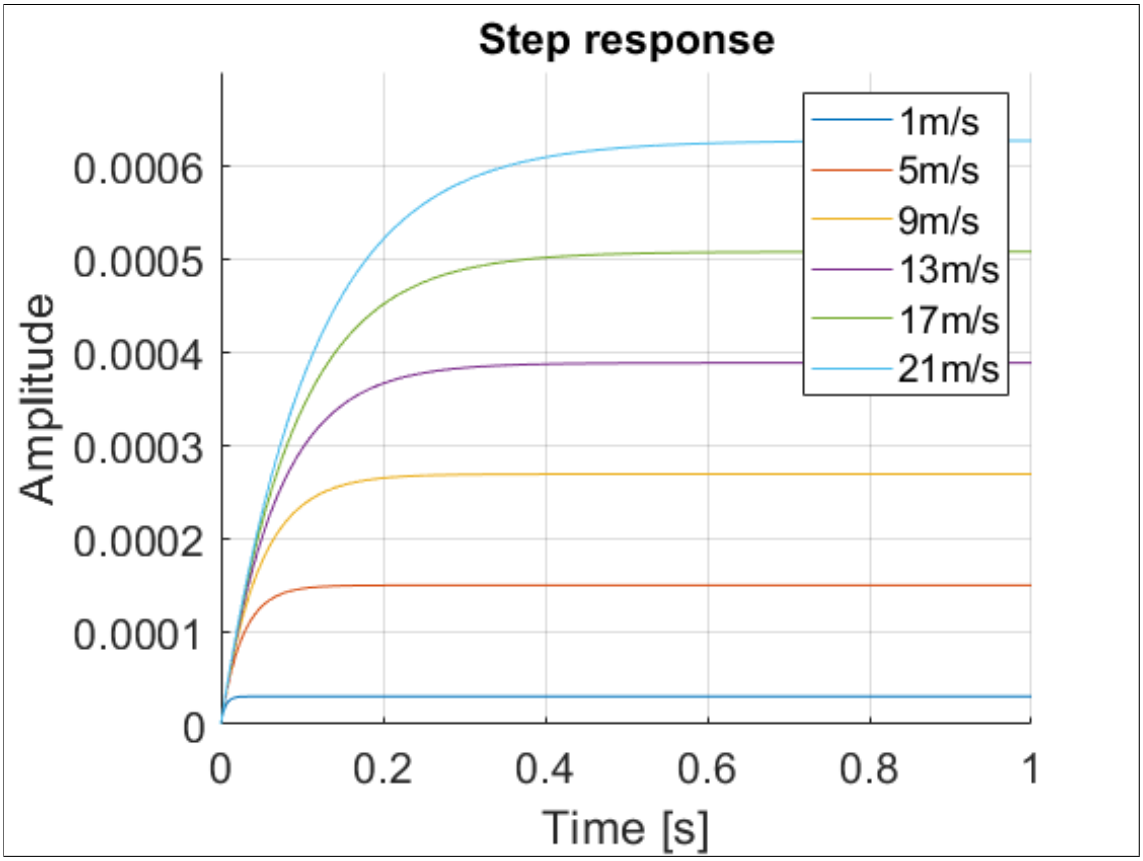

Figure 9: Step response of vehicle from yaw moment to yaw rate at different velocities

Figure 9 shows different amplitudes at various velocities. This means that the same yaw moment change at different velocities has different amplitudes.

Figure 10 shows the bode diagram of the system.

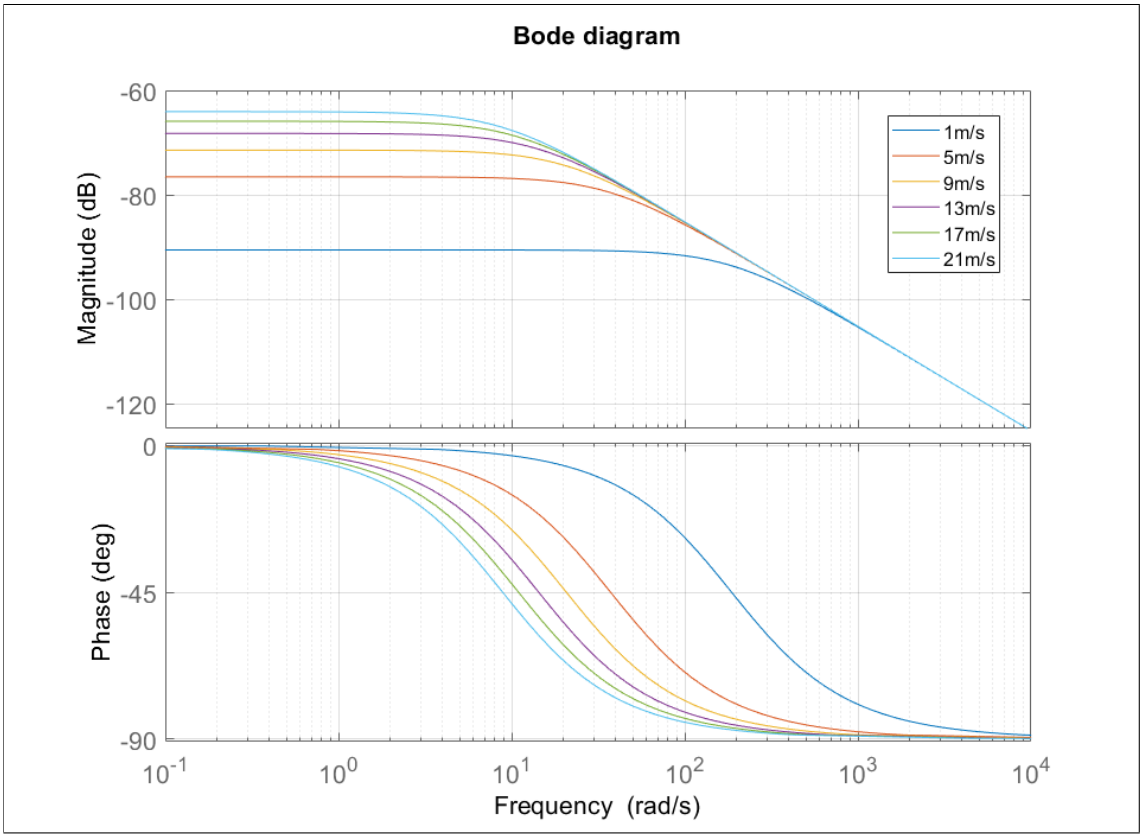

Figure 10: Bode plot of linear vehicle model at different longitudinal velocities

The bode diagram shows how the magnitude of the system increases as vehicle velocity is increasing. The vehicle velocity value has most significant influence on vehicle handling. As the bode diagram shows the vehicle can be controlled at full velocity range.

3.5 PID Controller

The PID controller may be easily implemented and it is often simple to tune to achieve acceptable results. PID get as input the error e between $\dot{\psi}_{reference}$ and current value $\dot{\psi}$.

$$e = \dot{\psi}_{reference} - \dot{\psi}_{actual} \tag{39}$$

From this follows that the error controller applies proportional, integral and derivative terms to calculate optimal output variable, which tries to drive error to zero.

$$u = K_P e + K_I \int e + K_D \frac{de}{dt} \tag{40}$$

where K_P, K_I, K_D are the PID coefficients for proportional, integral and derivative terms.

3.5.1 Requirements

PID controller was chosen because it is relatively easy to implement and it can fairly easily be tuned for acceptable performance. It can also compensate for unknown design parameters and disturbances. Downside of the PID controller is that it can only handle linear systems. To ensure the desired behavior few requirements were set for the PID controller were set according to [5, p. 203.]:

- Control loop must be stable
- Controller must be robust
- Controller must show specific accuracy
- Must be sufficiently damped
- Must be sufficiently fast.

3.5.2 Gain-Scheduling

As it can be seen in Figure 10, the system is not linear as velocity is varied and could not fulfill the requirements set above. For this reason, a gain-scheduled PID controller was used. This ensures that the controller is robust and accurate to different parameters and disturbances. The problem with non-linear controllers is, that they require a lot of tuning to achieve acceptable and good performance. The D-term was left off in the PID controller, as it can easily lead to unstable behavior, if it is not properly filtered. This means that the PID-controller was reduced to PI controller. The model was linearized at different operating points and after that controller was tuned at these points. To model at different velocities, a state space model of the vehicle was used. This was carried out in MATLAB/Simulink simulation environment. The controller was designed to have bandwidth of 62 rad/s and phase shift of 60 $^\circ$. Figure 11 shows tuned P gain at different

operating points of the vehicle model. Figure 12 shows tuned I gains at different operating points of the vehicle model. The neutral steering vehicle was selected as reference.

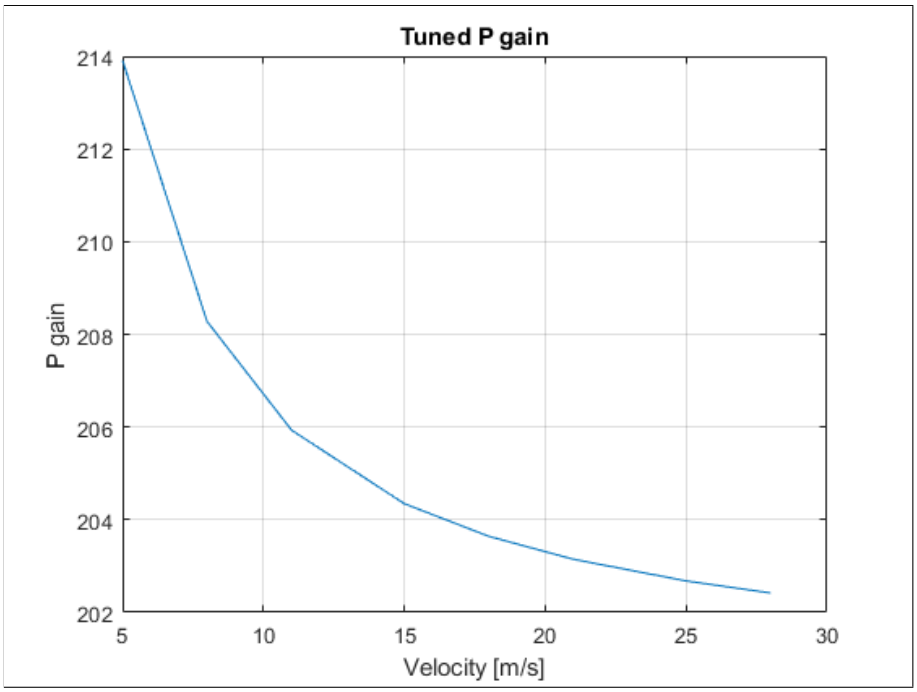

Figure 11: Scheduled P gains

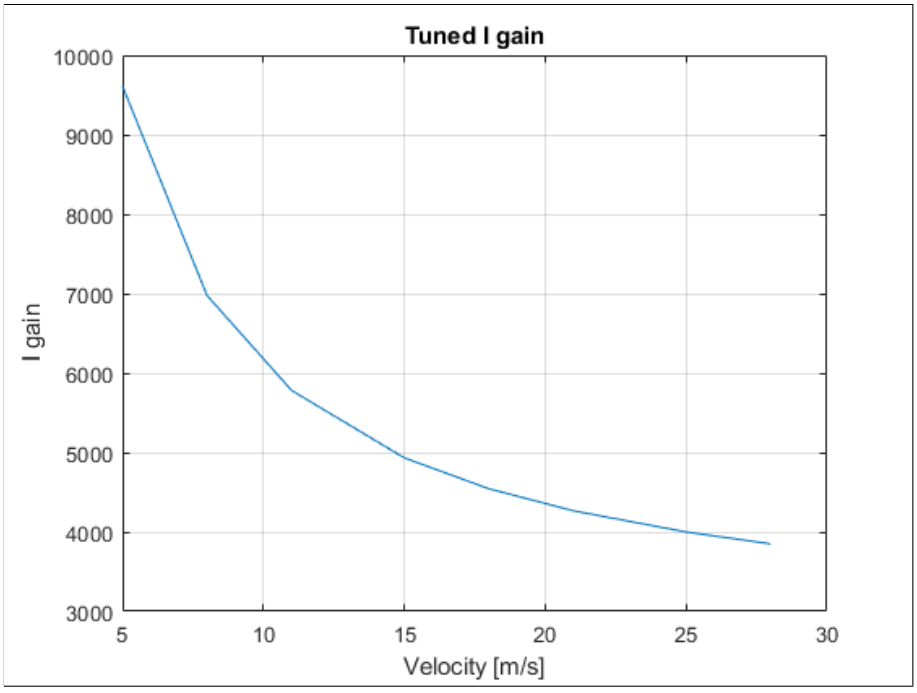

Figure 12: Scheduled I gains

These gains were tuned at different velocities and the average settling time of 0.1 was achieved. Maximum overshoot percentage was around 13 %. This overshoot is accept-

able as in our case the settling time is more important. Figure 13 shows vehicle yaw rate response to the step steer input of 65 ° with and without torque vectoring system.

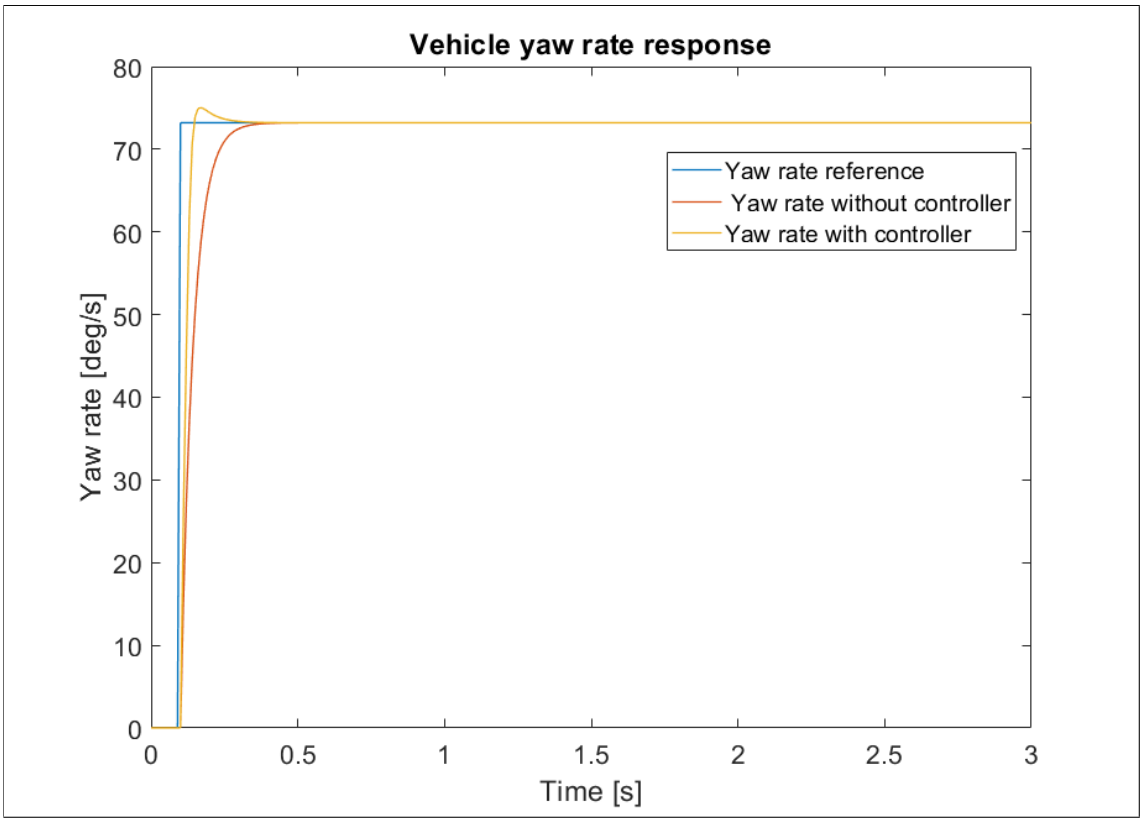

Figure 13: Vehicle yaw rate with and without controller at vehicle velocity of 11 m/s

In figure above it is shown that the vehicle with torque vectoring system responds faster to reference yaw rate but overshoots slightly at the end. The vehicle without torque vectoring system responds to steering input slower but does not overshoot. In the Metropolia Motorsport case faster response is always important as it allows the vehicle to change direction of travel more rapidly.

This yaw moment M_z produced by the PI controller is combined with yaw moment M_z produced by the feedforward controller. The feedforward controller allows to alter the vehicle's understeering or oversteering tendencies. The total yaw moment is given by the following equation:

$$M_{z_{total}} = M_{z_{PIcontroller}} + M_{z_{feedforward}} \tag{41}$$

This yaw moment is then distributed to wheel torques to achieve the desired yaw moment from the controller.

3.5.3 Wheel Torque Distribution

Yaw moment is laterally distributed between the left and the right wheels. This torque difference between the left and the right wheels creates additional yaw moment required by the controller. If the relationship between yaw moment and longitudinal tire forces is considered in seven DOF vehicle model the following equation can be written:

$$M_z = b_r F_{xrr} + b_f F_{xfr} - b_f F_{xfl} - b_r F_{xrl} \tag{42}$$

This corresponds to the yaw moment created by the longitudinal forces of the tires. These tire forces can be given as the wheel torque divided by the tire dynamic rolling radius.

$$F_x = \frac{T_d}{R_e} \tag{43}$$

where Td is wheel driving torque and Re is wheel dynamic rolling radius.
By combining equations 42 and 43 they can be rearranged to get the following equation:

$$\Delta T_Q = \frac{M_{z_{total}} R_e}{2bG_r} \tag{44}$$

where ΔT_Q is torque difference, b is half of the track length at front or rear and M_z is vehicle yaw moment.

This torque difference corresponds to the difference which needs to be achieved to be able produce the desired yaw moment. This torque difference is translated to wheel torques by the following equations:

$$T_{q_{FL}} = T_d + \frac{1}{4}\Delta T_Q \tag{45}$$

$$T_{q_{FR}} = T_d - \frac{1}{4}\Delta T_Q \tag{46}$$

$$T_{q_{RL}} = T_d + \frac{1}{4}\Delta T_Q \tag{47}$$

$$T_{q_{RR}} = T_d - \frac{1}{4}\Delta T_Q \tag{48}$$

where Tq_D is driver asking torques, Tq_{FL}, Tq_{FR}, Tq_{RL} and Tq_{RR} is modified asking torques.

3.6 Front to Rear Torque Distribution

In four wheel drive vehicles torques can be also longitudinally distributed. This can be done to achieve better grip from the rear wheels at acceleration or to recover more energy during braking from the front wheels. This distribution can be done based on vertical tire forces of the vehicle. Static forces on axles are given by the following equations:

$$Fz_f = \frac{mgl_r}{l} \tag{49}$$

$$Fz_r = \frac{mgl_f}{l} \tag{50}$$

where Fz_f and Fz_r is static weight on the front and the rear axle. During acceleration, this weight transfer from one axle to another axle is based on centre of gravity height and acceleration value and it is given by the following equation:

$$\Delta fz = \frac{mha_x}{l} \tag{51}$$

where Δfz is the weight transfer as a result of longitudinal acceleration. Equations 49 and 50 are combined with equation 51 and can be rewritten as:

$$Fz_f = \frac{mgl_r}{l} - \frac{mha_x}{l} \tag{52}$$

$$Fz_r = \frac{mgl_f}{l} + \frac{mha_x}{l} \tag{53}$$

Front and rear axle weights are rewritten as a ratio between the front axle weight and the vehicle total weight:

$$\theta = \frac{fz_f}{fz_f + fz_r} \tag{54}$$

where θ is the weight ratio between the front axle and the vehicle.

Torque requested by the driver can be written as separate torque request for the front axle and the rear axle.

$$T_{df} = T_d + T_d \tag{55}$$

$$T_{dr} = T_d + T_d \tag{56}$$

where T_d is request torque by the driver for each electrical motor and Td_f, Td_r are total requested torque by the driver for the front and the rear axle. These requested torques at the front and the rear axle can be combined with the weight ratio to distribute total vehicle torque between the front and the rear axle by following equations:

$$T_{fl/fr} = \theta T_{df} \tag{57}$$

$$T_{rl/rr} = (1 - \theta) Tdr \tag{58}$$

where $T_{fl/fr}$, $T_{rl/rr}$ are modified torques to each wheel.

3.7 Functional Requirements

As this developed torque vectoring system is a prototype, fail safe systems are implemented to make sure that the system is safe to test and use. Also if the controller fails, the vehicle would be still stable and controllable. This ensures that if the vehicle system malfunctions during testing, no serious injuries would occur. For this reasons the following set of constraints were set for the torque vectoring system.

- Maximum yaw rate reference value - for safety reasons vehicle maximum yaw rate reference is limited by equation (40). This ensures that vehicle can realistically achieve desired yaw rate reference.
- Minimum vehicle speed 3 m/s - If vehicle velocity is lower than 3 m/s, torque vectoring will be inactive for safety reasons.
- Steering wheel angle $|\delta| < 8$ - If steering wheel angle is less than 8 degrees torque vectoring is inactive. This ensures vehicle longitudinal stability when no cornering is presented with vehicle.
- Pedal position < 0.05 - If acceleration pedal is pressed less than 5 % torque request is set to zero.
- Sensor values - If sensors values are out of valid and possible range, torque vectoring is turned off for safety reasons.

4 Traction Control System

The objective of the traction control system is to reduce excessive wheel slip. As it can be seen in figure 4 tire produces peak force at specific slip ratio value. If this slip ratio is exceeded, tire longitudinal performance in most cases is decreased. This usually can lead to decreased vehicle stability, steerability and excessive tire wear. By keeping wheel slip at an optimal level, it is possible to keep the tire at maximum traction.

4.1 Control Systems

Maintaining specific wheel slip is a hard task due to wheel dynamics being highly nonlinear, and also road-tire interaction has a lot of unknown and hard to measure parameters, which contributes to road-tire coefficient of friction. To reduce excessive wheel slip, many different controllers were developed for the traction control system. For HPF021 vehicle, two different controllers were developed to be used in the traction control system. The first system is velocity control, which restricts motor maximum rpm speed to maintain optimal wheel slip. The second controller is a fuzzy logic controller which takes an input wheel slip and derivative of wheel slip. Based on these inputs, the controller calculates optimal torque reducing coefficient. For reference slip value of 0.20 was chosen for the controllers. This is based on available tire data obtained from FSAE TTC. This reference value is a little bit higher than optimal slip ratio to achieve maximum longitudinal potential from tire. This is done so that the tire can always achieve its peak and is not over restricted by the traction control system.

4.1.1 Velocity Control

The first controller is a simple velocity controller. As each wheel is equipped with an electrical motor a maximum wheel speed can be set for each wheel based on the vehicle's current velocity and approximated tire radius.

$$\omega_{reference} = \frac{V_x}{Re} \tag{59}$$

where V_x is vehicle velocity and Re is dynamic radius of tire.

From this reference maximum allowed wheel speed can be calculated as follows:

$$\omega_{max} = \omega_{reference}(1 + \kappa_{reference}) \tag{60}$$

where $\kappa_{reference}$ is wheel slip reference.

Previous equation can be rewritten as a maximum speed set for motor:

$$Motor_{maxrpm} = \frac{\omega_{max} 30 Gr}{Re\pi} \tag{61}$$

where Gr is transmission gear ratio and Re is tire dynamic rolling radius.

$Motor_{maxrpm}$ is limited motor speed in rpm. This value is send then to inverters which restricts wheel speed if it surpasses limited motor speed. To make sure that this value does not exceed a possible motor speed it has to be bounded by maximum possible motor speed by the following equation:

$$Motor_{maxrpm} = \begin{cases} Motor_{maxrpm}, & if \quad Motor_{maxrpm} < Motor_{limit} \\ Motor_{limit}, & if \quad Motor_{maxrpm} > Motor_{limit} \end{cases} \tag{62}$$

4.1.2 Fuzzy Logic Control

Fuzzy control is based on rules which can be described in words. Fuzzy logic works nearly in the same way as the conventional logic except that in fuzzy logic, values can be anything between 0 and 1. Fuzzy logic is divided into three processes called fuzzification, rules

and defuzzification. Fuzzification turns verbal input into mathematical expression. This is done through membership functions. Every membership function has so called degree of membership. To connect input and output variables rules are set. In the deffuzification process the rules are translated into numerical values. Membership functions with high degree of membership affect output more than membership functions with small degree of membership functions [13, p. 27-30].

In the design of the fuzzy logic control two inputs were used: wheel slip and derivative of wheel slip respectively. In most traction control system literature only wheel slip is considered as an input variable. In this case wheel slip and derivative of wheel slip were used to achieve faster convergence to zero between actual wheel slip and reference wheel slip.

Figure 14 shows fuzzification of the wheel slip into membership functions which are ZO, PS, PM and PB respectively.

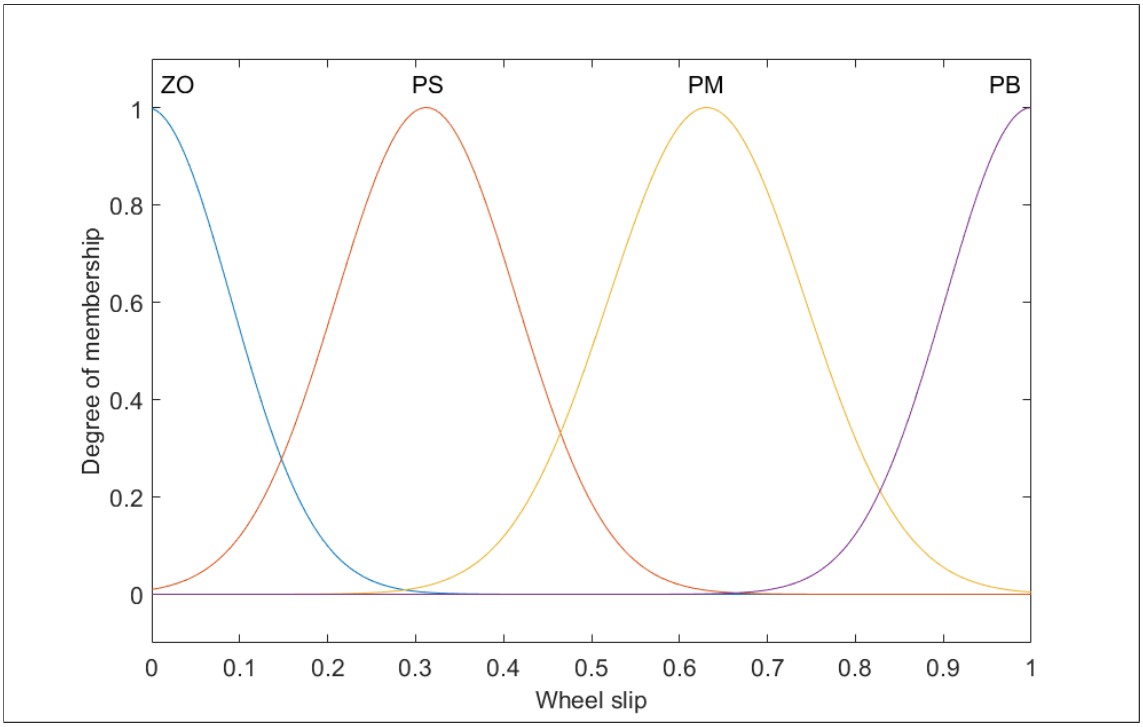

Figure 14: Surface view of fuzzy logic controller

Figure 15 shows fuzzification of the derivative of wheel slip into membership functions which are NB, NM, NS, ZO, PS, PM and PB

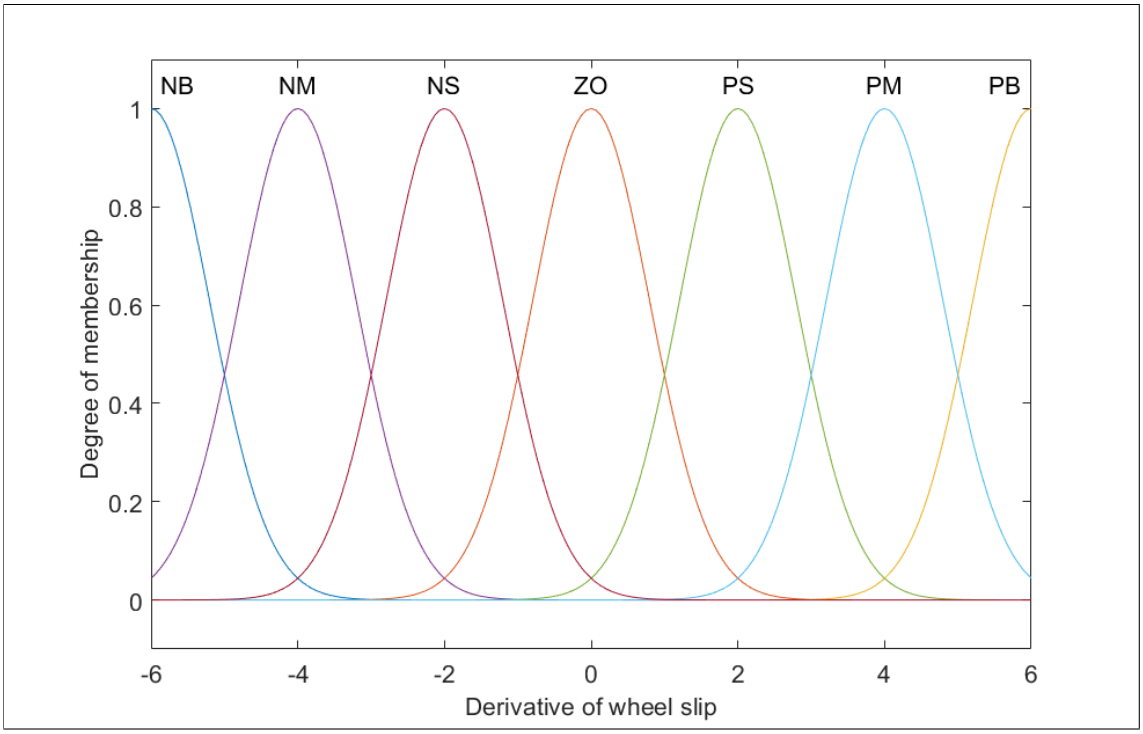

Figure 15: Surface view of fuzzy logic controller

These abbreviations stand for the following words:

- NB = negative big
- NM = negative medium
- NS = negative small
- ZO = zero
- PS = positive small
- PM = positive medium
- PB = positive big.

To tie these input values to output value a set of rules were created, based on current wheel slip and derivative of wheel slip. These rules can be seen in table 3.

Table 3: Rule base for traction control system

$\dot{\kappa}$ / κ	**Z0**	**PS**	**PM**	**PB**
NB	ZO	PS	PM	PB
NM	ZO	PS	PM	PB
NS	ZO	PS	PB	PB
ZO	ZO	PM	PB	PB
PS	ZO	PM	PB	PB
PM	ZO	PM	PB	PB
PB	ZO	PB	PB	PB

As it can be seen in the table if wheel slip value is zero, then the system should not alter wheel torque. As the wheel slip is increasing, the output value should be also increasing to reduce wheel torque to achieve optimal slip. This rule base takes also into account the derivative of wheel slip values, to reduce wheel torque as wheel slip is starting to increase. The idea of this is to proactively start reducing wheel torque to achieve smaller wheel slip values, than with only the wheel slip system.

Figure 16 shows a plotted surface view of the fuzzy logic controller. Output of the fuzzy logic controller is the required reducing torque coefficient.

Figure 16: Surface view of fuzzy logic controller

The plotted fuzzy logic surface shows a three-dimensional curve that represents mapping from input variables to an output variable. From this curve it can be seen that the curve follows rules set in table 3. Both control systems are implemented as Simulink models.

5 Simulations

As real vehicle testing on track was not possible at the time of the writing this thesis, two different simulation software were used to perform different tests for the controllers to ensure and guarantee vehicle lateral and longitudinal stability and to simulate controller preliminary performance. Both the torque vectoring and the traction control systems was tested in Simulink with the self-developed 7-DOF vehicle mode described previously. To further test these control systems, co-simulations with IPG Carmaker were also performed. The main objective of these simulations was to check, if these systems would bring benefit in simulations and to make sure that they are safe to test in the real vehicle. As this vehicle is a prototype and malfunction of these systems could easily lead to injuries or vehicle damages, it is important to test the control systems in a safe environment first.

5.1 MATLAB/Simulink

Simulink is a MATLAB extension, which adds graphical user interface to model, design and simulate dynamical systems. In Simulink systems are built with the help of block diagrams. These systems can be linear or nonlinear and they can be continuous or discrete systems or something in between of these two. It is possible to include also MATLAB scripts into the models. Simulink also supports code generation for designed systems. Simulink also offers model validation checks and systematic verifications for the models. To solve differential equations a lot of different solvers can be used from stiff to non-stiff solvers. This makes it ideal to solve complex differential equations. Simulink offers easy tuning methods for PID controllers and easy implementation of different controllers. These controllers can also be easily tested in Simulink simulation environment. This contributes to easy development and testing of different dynamical models which leads usually to faster development and shortens real world testing time.

5.2 IPG Automotive Carmaker

IPG Carmaker is widely used in the automotive industry. Carmaker offers a complete model environment with an intelligent driver model, a detailed vehicle model and flexible models for road and traffic. The software offers an easy test of realistic driving scenarios for different vehicle parameters. IPG Carmaker also offers easy integration with MATLAB/Simulink. A vehicle model with a driver is implemented in the IPG carmaker software. A control system is developed and driven in Simulink. All necessary quantities can be obtained inside Simulink for the control systems and output quantities are passed back to Carmaker to calculate vehicle states.

5.3 Traction Control System Simulations

As a real-world vehicle test was not possible to perform, the control systems were tested in a simulation environment. The traction control system was tested in Carmaker simulation software and Simulink simulation software. Throttle signal was implemented as a ramp input with rise time of 0.1 seconds from value 0 to 1. This test corresponds to an Acceleration event held at the competition. Objective of this test is to cover distance of 75 meters as fast as possible. Figure 17 shows vehicle wheel speeds and vehicle velocity during an acceleration test in Carmaker. The figure on the left corresponds to the acceleration test without the traction control system turned on and the right figure corresponds to an acceleration test with the traction control turned on. The vehicle traction control system is activated when vehicle velocity exceeds the traction control system activation value which is set to 2.5 m/s in this case. This is done because as the vehicle starts to move, wheel slip values can be high a short amount of time and could lead to unnecessary traction control system activation.

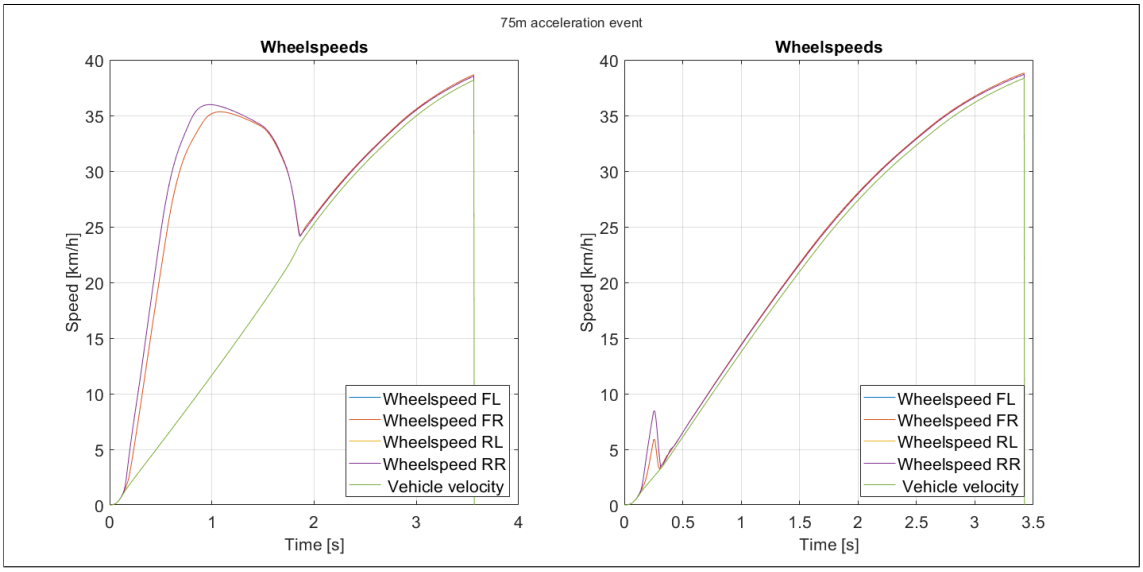

Figure 17: Acceleration test implemented in Carmaker

As the figure above shows, when traction control system is not enabled, wheel speeds are exceeding greatly vehicle velocity. This means that wheels are slipping, and tire full potential is not used to maximum according to tire FX-SR curve. At some point in the acceleration test, when each wheel vertical tire force is increasing usually due to aerodynamic downforce and higher power requirements for keeping vehicle acceleration, the tire is able to transmit more longitudinal force, thus reducing slip and increasing vehicle longitudinal performance. The figure on the right shows that when the traction control system is enabled, wheel slip can only be seen at the start of the acceleration event. After activation velocity wheel torque is restricted to keep the wheel slip at an optimal level of tire FX-SR curve. In these simulations wheel slip reference of 10 % was chosen. According to the simulation the total time to complete the acceleration event without traction control system was 3.57 seconds. When the traction control system was turned on, the total time to complete the acceleration event was 3.42 seconds.

Figure 18 shows same acceleration event test performed with the self-developed 7-DOF vehicle model. The figure on the left corresponds to the acceleration event test without the traction control system and the right figure corresponds to test with the traction control system turned on.

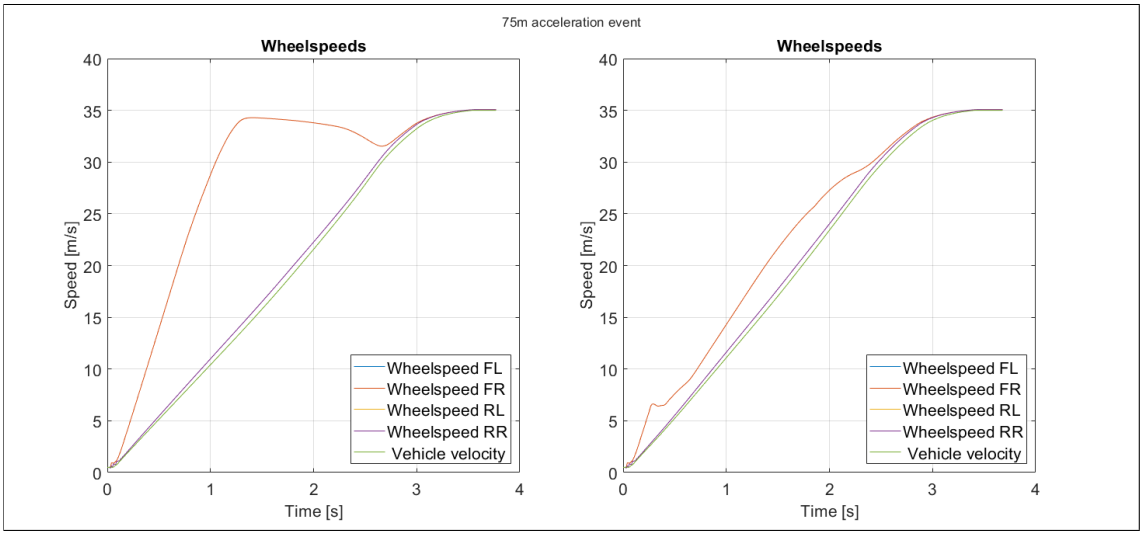

Figure 18: Acceleration test implemented in Simulink model

The figure on the left shows a big difference between front wheel speeds and vehicle velocity. This is usually due to a high load transfer from the front axle to the rear axle during acceleration. In this case as the vehicle's longitudinal acceleration is increasing, due to the load transfer the vertical tire forces of the front tires are decreasing and the rear tires vertical tire forces are increasing. This leads to a situation where the front tires can transmit less force than the rear tires which leads to more wheel slipping at the front wheels. In figure on the right the front wheel speeds are decreased by the traction control system. As the controller senses wheel slip, wheel torque is then reduced to reduce wheel slip to reference value.

Figure 19 shows wheel slips during the same Carmaker acceleration test as in the previous Carmaker figure. The figure on the left shows wheel slips without the traction control system and the right figure shows wheel slips with the traction control system.

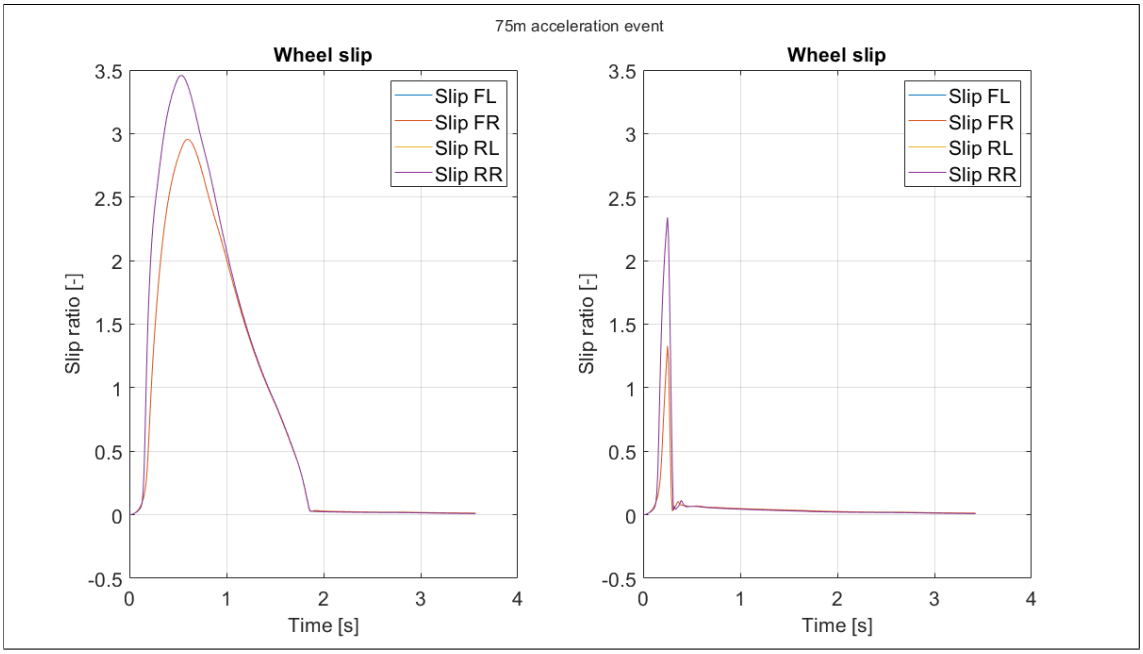

Figure 19: Wheel slips during acceleration test in Carmaker

As it can be seen in the figure without the traction control, wheel slip is not restricted to any value and is rising to its maximum peak. The rear wheels are slipping a little bit less than the front wheels during this acceleration event. The figure on the right shows that when the traction control system is turned, wheel slip is restricted after vehicle velocity surpasses activation velocity and is maintaining the desired wheel slip ratio to achieve maximum longitudinal performance from tires based on the tire FX-SR curve.

Figure 20 shows wheel slips during the acceleration event tested in Simulink. The left figure represents wheel slips without the traction control system and the right figure represents wheel slips with the traction control system.

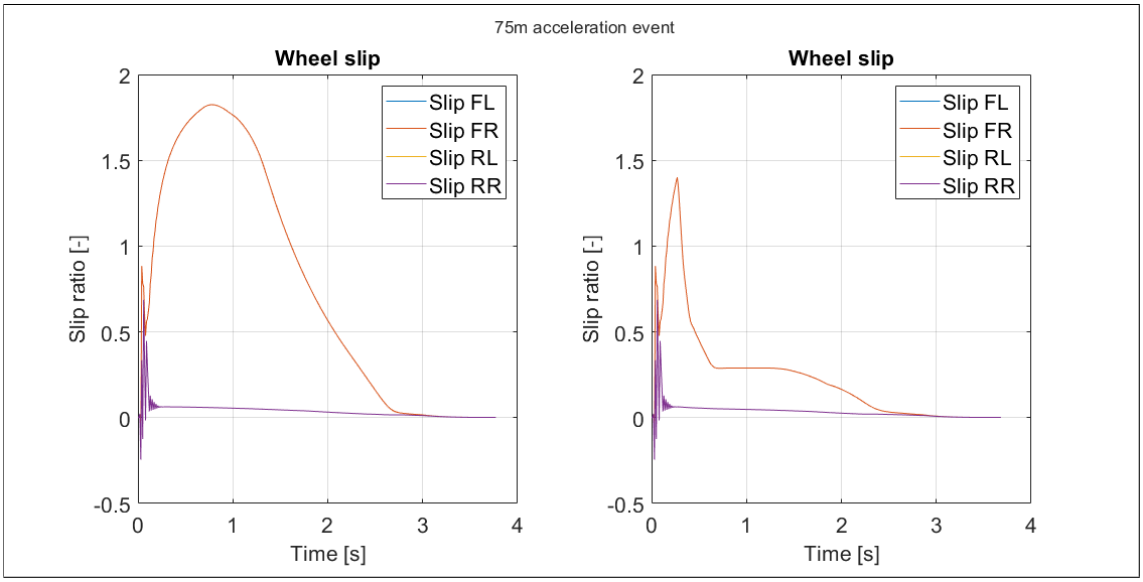

Figure 20: Wheel slips during acceleration test in Simulink

In the left figure the rear wheels are not slipping much compared to the front wheel slips. In this figure the front wheels are nearly slipping full time during the acceleration test. In the right figure when the traction control system is turned on, wheel slips which are occurring at front wheels are greatly reduced with the traction control system.

As the traction control system simulations in both Carmaker and Simulink show, it seems that acceleration times at the event are different from each other. This is due to different vehicle models used in simulations. The Carmaker uses MBS vehicle model to simulate vehicle behavior at the track and aerodynamic coefficients are mapped with this model more accurately. Simulink uses a model, which was described earlier in this thesis. The biggest difference comes from the tire model used in Carmaker and Simulink. In the Carmaker tire model with plotted data points were used. The Simulink model uses the simplified Pacejka model as a tire model. These are the differences, which lead to different acceleration event times measured in simulation software.

In both testing cases the traction control system showed improvement in the form of reducing wheel slip and increasing vehicle longitudinal performance. To further validate these results, a real testing on track would need to be performed to validate data obtained from the simulations.

5.4 Torque Vectoring System Simulations

The torque vectoring system was simulated with different events in Simulink and Carmaker. As the Simulink model did not have a driver model, which could follow the desired course, only a step response test with 7-DOF model was performed in Simulink. In the Carmaker slalom and autocross tests were performed to evaluate the vehicle's response and controller performance.

5.4.1 Step Response

The first test was vehicle response to step steer input at the constant longitudinal velocity of 11 m/s. During this test the steering wheel angle is turned 30° and stayed at that angle during the simulation. Figure 21 shows vehicle yaw rate during the step steer simulation. The blue line shows yaw rate reference which is calculated based on vehicle velocity and steering wheel angle. The orange line represents vehicle response without torque vectoring system. The yellow line represents vehicle response with the torque vectoring system turned on.

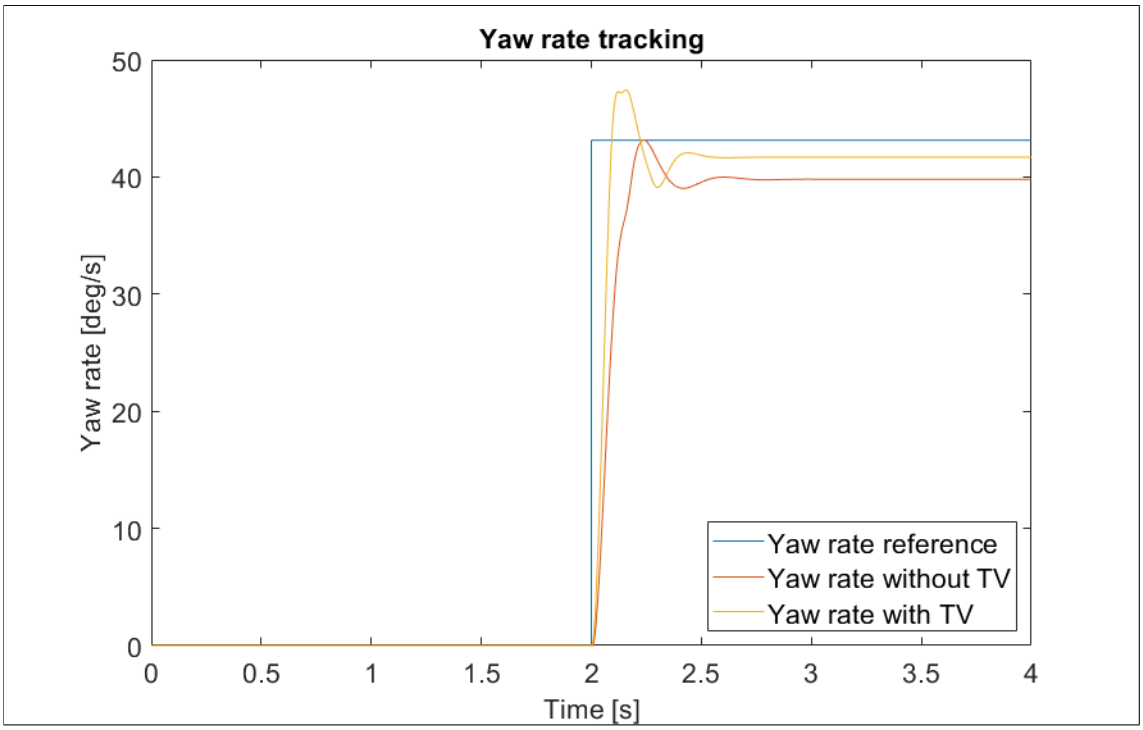

Figure 21: Yaw rate tracking during step steer simulation

Step response is actuated at two second's mark. The vehicle starts to follow the desired yaw rate with some delay depending on the vehicle's yaw inertia and yaw moment. The vehicle with a torque vectoring system reacts faster to yaw rate reference. This leads to a higher overshoot value than with the vehicle without the torque vectoring system. The vehicle with the torque vectoring system has also shorter settling time when compared to the vehicle without the torque vectoring system. In both cases there is still a steady state error presented. In case of the vehicle with torque vectoring system this steady state error can be manipulated to have the vehicle with understeering or oversteering tendencies.

Figure 22 shows a tracked yaw rate error during the step steer test. The blue line represents an error between the vehicle without a torque vectoring system and yaw rate reference. The orange line represents an error between the vehicle with a torque vectoring system and yaw rate reference.

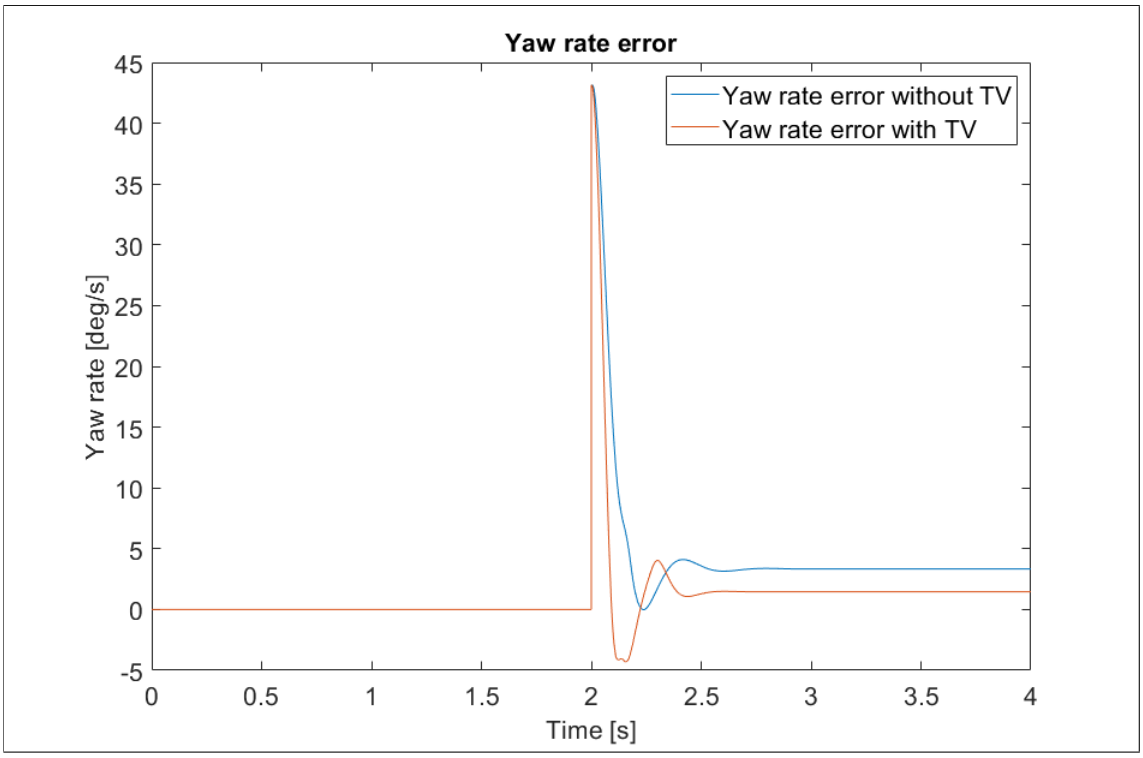

Figure 22: Yaw rate error during step steer simulation

In case of a vehicle with a torque vectoring system, the vehicle responds faster to yaw rate error and drives faster to zero with some steady state error. The vehicle without a torque vectoring system responds slower to yaw rate error and is left with higher steady state error.

5.4.2 Slalom

The first test performed in Carmaker was a slalom test. The objective of the vehicle is to drive with zigzag maneuver around cones. This test is performed to see the vehicle's transient response. Figure 23 shows yaw rate during the slalom test. The top figure represents the slalom test without the torque vectoring system and the bottom figure represents the test with torque vectoring.

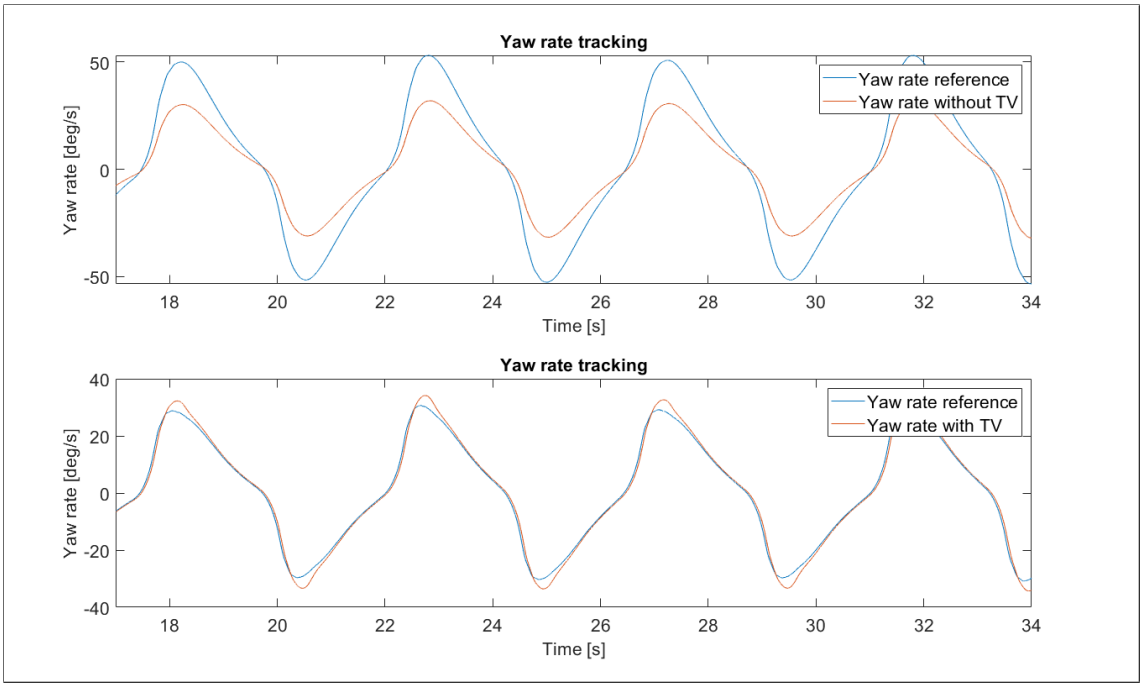

Figure 23: Yaw rate tracking during slalom test

As it can be seen in the test without the torque vectoring system, the vehicle is not able to achieve reference yaw rate requested by the driver. The, vehicle's yaw rate also follows the reference yaw rate with delay due to inertia and the tire lateral build up properties. From test with torque vectoring, it can be seen that the vehicle follows a closer reference yaw rate and is able to achieve these values and even crosses the yaw rate reference values. These test also show that the driver with the torque vectoring system needs to turn the steering wheel less, as the vehicle is following and responding to the driver inputs faster when compared to the vehicle without torque vectoring system.

Figure 24 shows the yaw rate error during the slalom test. The top figure represents the yaw rate error in the vehicle without the torque vectoring system and the bottom figure

represents the vehicle with the torque vectoring system.

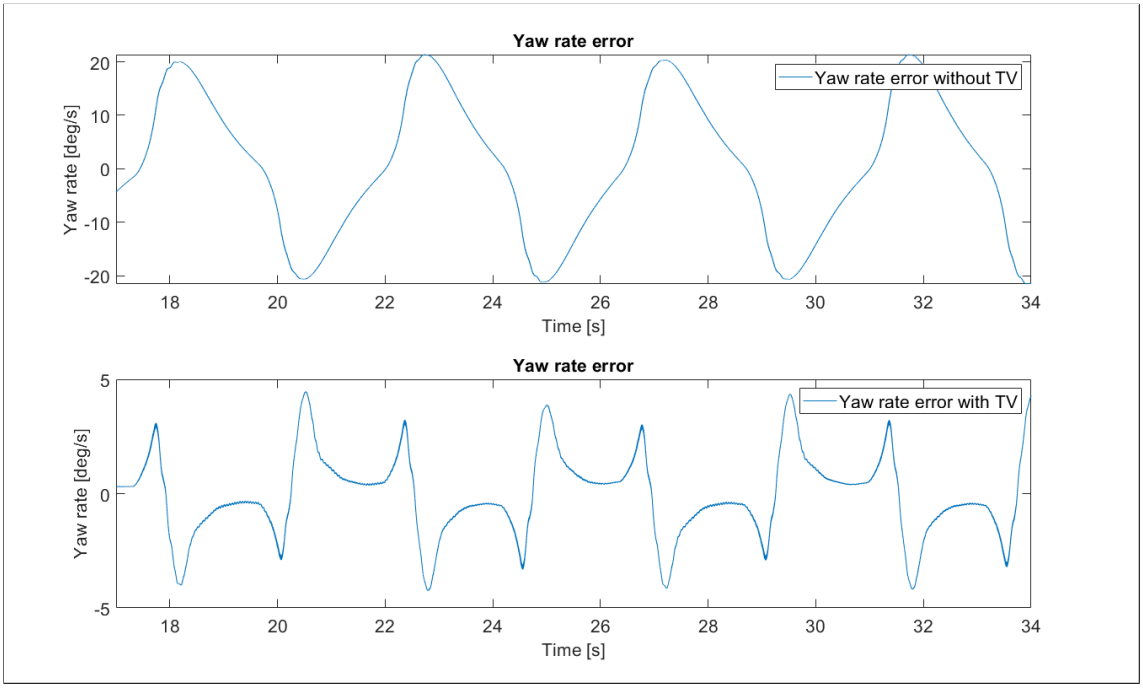

Figure 24: Yaw rate error during slalom test

In these figures it can be seen that the error between the reference yaw rate and the yaw rate is smaller in the vehicle with the torque vectoring system. This leads to better handling of the vehicle as the vehicle is following better driver inputs.

5.4.3 Autocross

To simulate the torque vectoring system as closely as possible to the real test an Autocross test was carried out. This test represents Autocross discipline in competitions. The objective of this test was to drive one lap around the track as fast as possible.
Figure 25 shows yaw rate during the Autocross test. The top figure represents the Autocross test without the torque vectoring system and the bottom figure represents the test with the torque vectoring system.

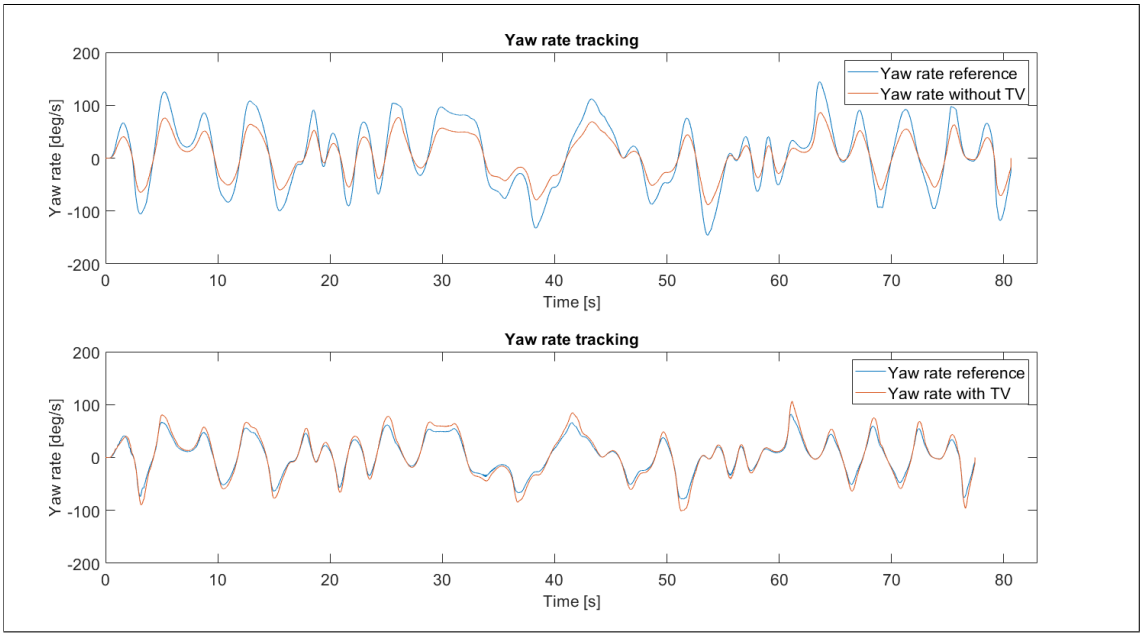

Figure 25: Yaw rate tracking during Autocross test

In these figures it can be clearly seen that the vehicle with the torque vectoring system is tracking much better yaw rate reference requested by the driver. Also yaw rate reference is decreased in case of the vehicle with the torque vectoring due to faster vehicle response. This also leads to increased vehicle's performance and faster times around the lap, which can be seen in the figure above.

Figure 26 shows the yaw rate error between reference yaw rate and actual yaw rate. The top figure represents the vehicle without the torque vectoring system and the bottom figure represents the vehicle with the torque vectoring system.

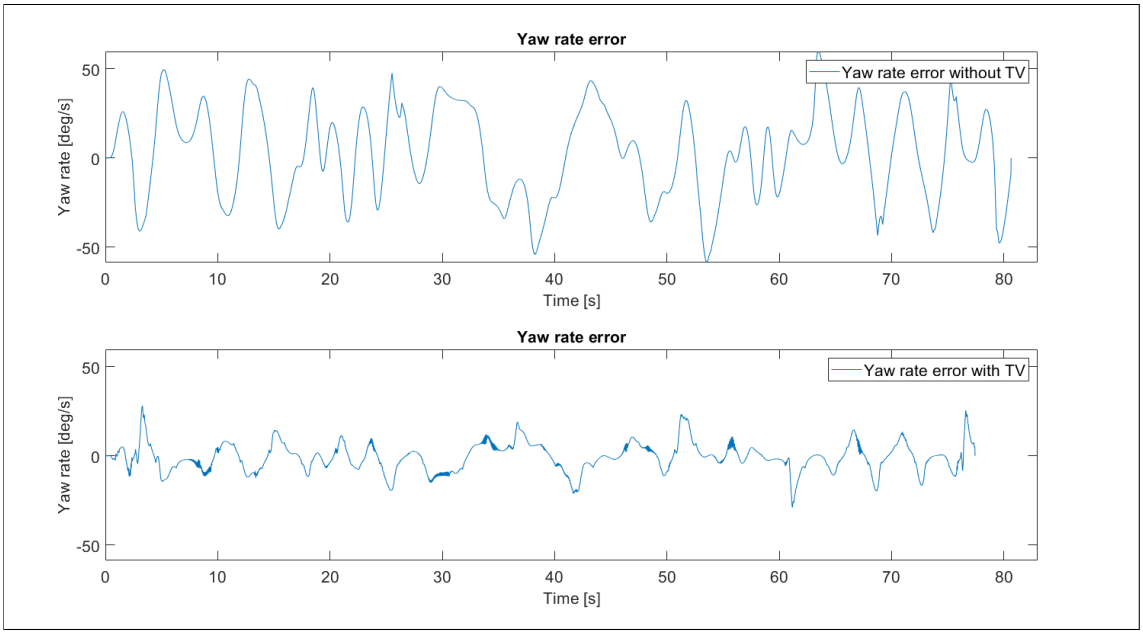

Figure 26: Yaw rate error during Autocross test

Based on the figure above it can be seen that the yaw rate error is reduced greatly when compared to the vehicle without the torque vectoring system. In the bottom figure peaks can be seen in some places of the data. This is usually due to the vehicle oversteering which requires the driver to reduce the steering wheel angle to eliminate excessive oversteering behavior.

Figure 27 shows slip angle during the Autocross event. The top figure represents the vehicle without the torque vectoring system and the bottom figure represents the vehicle with the torque vectoring system. Slip angle contributes to the vehicle's handling and stability. With high slip angle values the vehicle is said to be unstable and is harder to control for the driver.

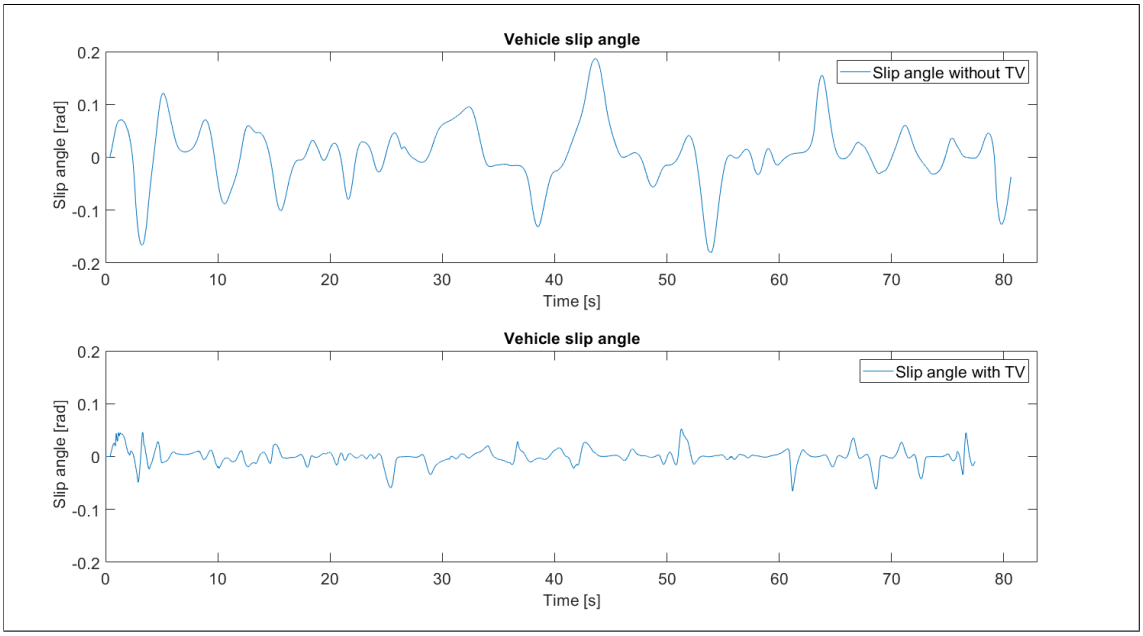

Figure 27: Yaw rate error during step steer simulation

The figure above shows smaller slip angle values in the vehicle with the torque vectoring system. This usually increases the vehicle's stability and the vehicle is easier to control. In the vehicle with the torque vectoring system, slip angle peaks are much sharper and direction change is much faster.

Based on the performed simulations, the vehicle showed improvements with both torque vectoring and traction control systems. To further test and validate these control systems real testing would need to be performed. In this case real testing was not possible to perform and simulations were the only available way to evaluate the controller and the vehicle performance.

6 Conclusions

Both traction control system and torque vectoring were developed for the Metropolia Motorsport vehicle. The torque vectoring system was designed to use gain-scheduled PI controller and feedforward controller to drive the yaw rate difference between reference and actual value to zero. The traction control system was designed to use two different controllers, fuzzy logic controller and velocity controller to control wheel slip. To test these systems and simulate vehicle behavior, a 7-DOF vehicle model was developed and implemented in MATLAB's Simulink interface. As the development of the vehicle was rather late and it was not possible to make any validation of the vehicle model a decision was made to use IPG Carmaker software to simulate the control systems as it offers a ready-made driver model, which can somehow represent a real driver on the track.

These systems were tested in different tests. The traction control system was tested as an acceleration event which was held at the competition. The idea of this test was to cover the distance of 75m as fast as possible. The torque vectoring system was tested as a step steer input, constant turn, slalom and lastly autocross event to evaluate the performance of this controller. The traction control system showed improvement in form of less tire slip and wheel speed was also reduced. In simulations this leads to faster acceleration time, and thus, increases the vehicle's longitudinal performance.

Although based on the simulations both systems showed increased vehicle performance, real world testing would still need to be carried out to validate and fine tune the controllers. Usually in a simulation environment it is hard to simulate noise and disturbances, which can occur in an electric vehicle from for example inverters, motors, suspension dynamics or tire dynamics. These noises and disturbances could create additional challenges when these control systems will be tested in the real vehicle.

To improve the vehicle's lateral dynamics, the torque vectoring controller can be expanded from a yaw rate tracking controller to track vehicle slip angle. The slip angle also plays a crucial role in the vehicle's steerability and stability. Measuring slip angle is usually a difficult task and requires measuring the vehicle's lateral and longitudinal velocities through

an optical sensor. In most cases slip angle is estimated with the help of Extended Kalman filter [14]. In this thesis road-tire friction was estimated to remain constant. This is usually not true as this friction changes a lot during driving and depends on many parameters. To achieve better yaw tracking and limit controller in low friction situations, more realistic tire model should be also implemented to estimate road-tire friction.

Bibliography

1 Formula Student Rules 2020. Formula Student Germany; 2019. Available from: https://www.formulastudent.de/fileadmin/user_upload/all/2020/rules/FS-Rules_2020_V1.0.pdf [cited March 25, 2021].

2 Dieter Schramm, Manfred Hiller, Roberto Bardini. Vehicle Dynamics: Modeling and Simulation. Duisburg: Springer-Verlag Berlin Heidelberg; 2014.

3 Berntorp K, Olofsson B, Lundahl K, Nielsen L. Models and methodology for optimal trajectory generation in safety-critical road–vehicle manoeuvres; 2014. Available from: https://doi.org/10.1080/00423114.2014.939094.

4 Katz, Joseph. Race Car Aerodynamics, Designing for Speed. Cambridge, MA: Bentley Publishers; 2006.

5 Robert Bosch GmbH. Automotive Handbook, 10th Edition. Wiley; 2018.

6 Bakker E, Nyborg L, Pacejka HB. Tyre Modelling for Use in Vehicle Dynamics Studies. SAE International; 1987. Available from: https://doi.org/10.4271/870421.

7 Brach R, Brach M. The Tire-Force Ellipse (Friction Ellipse) and Tire Characteristics. SAE International; 2011. Available from: https://doi.org/10.4271/2011-01-0094.

8 Hans B Pacejka. Tire and Vehicle Dynamics, Third editions. Great Britain: Elsevier Ltd; 2012.

9 Mastinu G, Ploechl M. Road and Off-Road Vehicle System Dynamics Handbook; 2013.

10 Kaiser G. Torque Vectoring - Linear Parameter-Varying Control for an Electric Vehicle; 2015. Available from: http://tubdok.tub.tuhh.de/handle/11420/1230.

11 Jaafari S, Shirazi H. A comparison on optimal torque vectorin strategies in overall performance enhancement of a passenger car; 2016.

12 R Rajamani. Vehicle Dynamics and Control Second Edition. Boston: Springer, Boston, MA; 2012.

13 Zetterqvist C. Powertrain modelling and control algorithms for traction control. Linköping University, Department of Electrical Engineering; 2007. Available from: http://urn.kb.se/resolve?urn=urn:nbn:se:liu:diva-10048.

14 Huang Y, Bao C, Wu J, Ma Y. Estimation of Sideslip Angle Based on Extended Kalman Filter car; 2017. Available from: https://doi.org/10.1155/2017/5301602.